AD-A191 544 COMPUTATION OF THE TURBULENT BOUNDARY LAYER DOWNSTREAM OF VORTEX GENERATORS(U) DAVID TAYLOR RESEARCH CENTER BETHESDA MD P K CHANG DEC 87 DTRC-87/054 1/1

UNCLASSIFIED F/G 20/4 NL

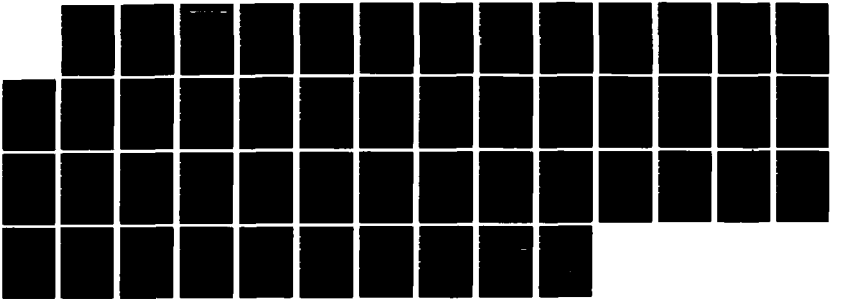

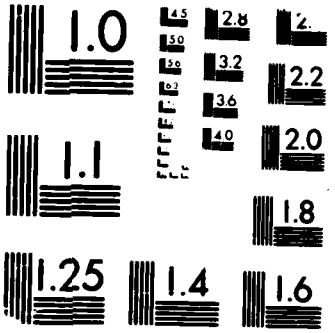

(4)

David Taylor Research Center
Bethesda, MD 20084-5000

DTRC-87/054 December 1987

Aviation Department
Research and Development Report

Computation of the Turbulent Boundary Layer Downstream of Vortex Generators

by
Paul K. Chang

DTRC-87/054 Computation of the Turbulent Boundary Layer Downstream of Vortex Generators

MAJOR DTRC TECHNICAL COMPONENTS

CODE 011 DIRECTOR OF TECHNOLOGY, PLANS AND ASSESSMENT

12 SHIP SYSTEMS INTEGRATION DEPARTMENT

14 SHIP ELECTROMAGNETIC SIGNATURES DEPARTMENT

15 SHIP HYDROMECHANICS DEPARTMENT

16 AVIATION DEPARTMENT

17 SHIP STRUCTURES AND PROTECTION DEPARTMENT

18 COMPUTATION, MATHEMATICS & LOGISTICS DEPARTMENT

19 SHIP ACOUSTICS DEPARTMENT

27 PROPULSION AND AUXILIARY SYSTEMS DEPARTMENT

28 SHIP MATERIALS ENGINEERING DEPARTMENT

DTRC ISSUES THREE TYPES OF REPORTS:

1. **DTRC reports, a formal series,** contain information of permanent technical value. They carry a consecutive numerical identification regardless of their classification or the originating department.

2. **Departmental reports, a semiformal series,** contain information of a preliminary, temporary, or proprietary nature or of limited interest or significance. They carry a departmental alphanumerical identification.

3. **Technical memoranda, an informal series,** contain technical documentation of limited use and interest. They are primarily working papers intended for internal use. They carry an identifying number which indicates their type and the numerical code of the originating department. Any distribution outside DTRC must be approved by the head of the originating department on a case-by-case basis.

NDW-DTNSRDC 5602/30 (Rev 11-87)

UNCLASSIFIED
SECURITY CLASSIFICATION OF THIS PAGE

REPORT DOCUMENTATION PAGE

1a. REPORT SECURITY CLASSIFICATION Unclassified	1b. RESTRICTIVE MARKINGS
2a. SECURITY CLASSIFICATION AUTHORITY	3. DISTRIBUTION / AVAILABILITY OF REPORT Approved for public release; distribution is unlimited.
2b. DECLASSIFICATION / DOWNGRADING SCHEDULE	
4. PERFORMING ORGANIZATION REPORT NUMBER(S) DTRC–87/054	5. MONITORING ORGANIZATION REPORT NUMBER(S)
6a. NAME OF PERFORMING ORGANIZATION David Taylor Research Center 6b. OFFICE SYMBOL (If applicable) Code 0113	7a. NAME OF MONITORING ORGANIZATION Aero Report 1302
6c. ADDRESS (City, State, and ZIP Code) Bethesda, MD 20084-5000	7b. ADDRESS (City, State, and ZIP Code)
8a. NAME OF FUNDING / SPONSORING ORGANIZATION 8b. OFFICE SYMBOL (If applicable)	9. PROCUREMENT INSTRUMENT IDENTIFICATION NUMBER
8c. ADDRESS (City, State, and ZIP Code)	10. SOURCE OF FUNDING NUMBERS PROGRAM ELEMENT NO. 611524N; PROJECT NO.; TASK NO. ZR0000101; WORK UNIT ACCESSION NO

11. TITLE (Include Security Classification)
Computation of the Turbulent Boundary Layer Downstream of Vortex Generators

12. PERSONAL AUTHOR(S)
Chang, Paul K.

13a. TYPE OF REPORT	13b. TIME COVERED	14. DATE OF REPORT (Year, Month, Day)	15. PAGE COUNT
Final	FROM 0986 TO 0987	1987 December	49

16. SUPPLEMENTARY NOTATION

17. COSATI CODES			18. SUBJECT TERMS (Continue on reverse if necessary and identify by block number)
FIELD	GROUP	SUB-GROUP	Boundary layer computations Flow separation Vortex generators

19. ABSTRACT (Continue on reverse if necessary and identify by block number)

The approximate analysis of three-dimensional incompressible turbulent boundary layer downstream of vortex generators is presented. Extensive numerical computations are carried out to assess the effectiveness of single-row, counter-rotating vane-type vortex generators to alleviate flow separation. Flow separation lines downstream of the vortex generators on a thick airfoil are determined in terms of size, location, and arrangement of the vortex generators. These lines are compared with the separation line without the vortex generators. High efficiency is obtained with the moderately slender rectangular blade of the generator. The results indicate that separation is alleviated more effectively in the region closer to the symmetry axis of the generator than in the outer region of the symmetry axis. No optimum conditions for the alleviation of flow separation are established in this investigation, and no comparisons are made with other analytical results and experimental data.

20. DISTRIBUTION / AVAILABILITY OF ABSTRACT ☒ UNCLASSIFIED/UNLIMITED ☐ SAME AS RPT ☐ DTIC USERS	21. ABSTRACT SECURITY CLASSIFICATION Unclassified
22a. NAME OF RESPONSIBLE INDIVIDUAL David D. Moran	22b. TELEPHONE (Include Area Code) (301) 227-1275 22c. OFFICE SYMBOL Code 0113

DD FORM 1473, 84 MAR — 83 APR edition may be used until exhausted. All other editions are obsolete.

SECURITY CLASSIFICATION OF THIS PAGE
UNCLASSIFIED

CONTENTS

FIGURES

NOMENCLATURE

A^*	Van Driest damping factor
C_f	Local skin friction coefficient
C_m	Constant for determining the grid size in y-direction
c	Chord length of airfoil
c_v	Chord length of vortex generator
D	Distance between two blades of the same configuration
d	Distance between two blades which form a divergent pair or distance between initial vortex cores
H	Shape factor of boundary layer ($= \delta^*/\theta$)
h	Height of vortex generator core
h_v	Height of vortex generator blade
h_x, h_y, h_z	Metric coefficient in the corresponding coordinate system
p	Static pressure
Re_c	Reynolds number ($= U_\infty c/\nu$)
s	Physical distance along streamline direction
s_u	Upper surface length of airfoil
U,W	Boundary-layer outer edge velocity component in x and z direction
u,v,w	Velocity components in boundary layer along x,y,z direction
u^*	Wall shear velocity ($= \sqrt{\tau_w/\rho}$)
x,y,z	Surface orthogonal coordinates
w_z	Derivative of w with respect to z

NOMENCLATURE (Continued)

α	Angle of attack, outer edge — viscosity coefficient
α_v	Incident angle of the vortex generator
Γ	Vortex strength
γ	Constant for determining grid size in y-direction for turbulent flow
γ_{tr}	Intermittency factor in the transition region
δ	Thickness of boundary layer
δ^*	Displacement thickness of boundary layer
ε	Eddy-viscosity
θ	Momentum thickness of boundary layer
ν	Kinematic viscosity
ρ	Density of fluid
τ	Shear stress

Subscripts

s	Streamline direction
v	Vortex generator
w	Wall
∞	Undisturbed flow region

Superscripts

–	Dimensionless quantity, except u, v, and w
'	Variable quantity with respect to chord direction

ABSTRACT

The approximate analysis of three-dimensional incompressible turbulent boundary layer downstream of vortex generators is presented. Extensive numerical computations are carried out to assess the effectiveness of single-row, counter-rotating vane-type vortex generators to alleviate flow separation. Flow separation lines downstream of the vortex generators on a thick airfoil are determined in terms of size, location, and arrangement of the vortex generators. These lines are compared with the separation line without the vortex generators. High efficiency is obtained with the moderately slender rectangular blade of the generator. The results indicate that separation is alleviated more effectively in the region closer to the symmetry axis of the generator than in the outer region of the symmetry axis. No optimum conditions for the alleviation of flow separation are established in this investigation, and no comparisons are made with other analytical results and experimental data.

ADMINISTRATIVE INFORMATION

Dr. Paul K. Chang, professor emeritus of the Catholic University of America, Washington, DC, is presently an invited professor of the Korea Advanced Institute of Science and Technology at Seoul, Korea. Dr. Chang conducted the analysis of three-dimensional incompressible flow downstream of vortex generators while a resident research associate sponsored by the National Research Council and funded by the David Taylor Research Center (DTRC) Independent Research Program.

ACKNOWLEDGMENT

Dr. Chang wishes to acknowledge Dr. D.D. Moran, Dr. H.R. Chaplin, and Mr. M.R. Schopper of DTRC and Mr. Ki Chung Sung of Korea for their assistance and support of this research.

INTRODUCTION

Structural considerations require the root cross-sections of large aspect ratio wings to be thick. Flow over such a thick airfoil section is characterized by a rapid pressure rise toward the trailing edge, and this large adverse pressure gradient causes the boundary layer to separate from the surface of the wing. The resulting stall is generally, undesirable, and therefore it is necessary to alleviate the flow separation. Among the various methods of suppressing flow separation is the use of vortex generators, which has been found to be relatively effective and simple.

Many types of vortex generators have been experimentally investigated from time to time. Schubauer and Spangenberg[1] presented 10 different shapes in their 1960 survey. In the present analyses, the flow field of a geometrically simple vane-type vortex generator is investigated.

Since the vortex generator flow field on a wing is three-dimensional and turbulent, the three-dimensional incompressible turbulent boundary-layer equations are analyzed by extensive numerical computation. Several parameters are investigated, including the length of a vane, the width between opposite vanes, the chord and height of a vane, and the locations of the vortex generators. The separation lines downstream of the vortex generators are determined to assess the extent of the flow separation alleviated by the vortex generators.

A survey of the literature has shown that investigations of the vortex generator flow field are limited. The following researchers are among those who have conducted investigations of vortex generator flow fields:

- Brown (1947)[2] investigated the induced velocity field of a vortex generator and prevented separation in the inlet diffuser of an aircraft engine by using a vortex generator.
- Jones (1957)[3] investigated the vortex path of a wing-type vortex generator and evaluated the vortex strength of the generator using potential flow methods.
- Schubauer and Spangenberg (1960)[1] measured the boundary-layer characteristics of various vortex generator flow fields showing the mixing of the high velocity outer layer with the low velocity inner layer.
- Pearcey (1961)[4] and Gartling (1970)[5] investigated the effects of vortex generators on flow separation alleviation at transonic speeds.
- Gartling (1970)[5] also studied the vortex-generator flow at supersonic speeds.
- Senoo and Nishi (1974)[6] carried out experiments for conical diffuser flow separation alleviation at divergence angles of 8, 12, 16, 20 and 30 deg for an area ratio of 4 using a variety of blade arrangements, inlet boundary-layer thicknesses and locations of vortex generators. The results showed that the vortex generator prevents flow separation up to a 16-deg divergence angle and that the pressure recovery is approximately equal to that of the best conventional conical diffuser. At blade setting angles of 14-16 deg, the best pressure recovery is achieved and larger aspect ratio blades were the most efficient. At a nominal diffuser divergence angle of 8 deg, pressure recovery is not affected by an increase in vortex generator number; at 16 deg, pressure recovery remains the same in spite of an increase in the vortex generator number beyond 10.
- Rousseau (1984)* carried out a limited experimental investigation of vortex generators attached to a thick airfoil.
- Nickerson (1986)[7] studied vortex generator flow at low Reynolds numbers.
- Greene (1986)[8] modeled the decay of a wing tip vortex in the atmosphere in a wake downstream of a wing in the atmosphere and found that typical vortex wake decay is caused by flow instability (vortex pair linking) except under strong stratified conditions.
- Lee (1986)[9] analyzed two-dimensional vortex generator flow and showed that flow separation can be prevented on a thick airfoil.

*Investigation by D.G. Rousseau, DTNSRDC/TM-16-84/03.

FLOW FIELD AFFECTED BY VORTEX GENERATORS

Examples of various vane-type vortex generators such as co-rotating, biplane, and counter-rotating vortex generato: , are shown in Fig. 1. Of these vortex generators, the counter-rotating vane-type generators are considered in the present analysis. The specific arrangement and nomenclature are shown in Fig. 2.

Figure 3 shows the line vortices of strength Γ in the y-z plane. These line vortices correspond to the tip vortices originating at the tip of the rectangular plate vortex generators which are at angle of attack to the upstream flow. Since the incident angle considered in the present report is less than 35 deg, the tip vortices are steady, and the vortex lines follow the streamlines (see Lugt,[10] p. 81). The counter-rotating tip vortex lines of equal vortex strength are straight and parallel to each other (Lugt,[10] p. 38). Jones (1957)[3] and Widnall (1975)[11] also indicate that the tip vortex lines are straight and parallel to each other in the x-z plane and prevail a considerable distance downstream. Jones (1957)[3] studied the vortex path of the counter-rotating vortex generator and indicated that the vortex first approaches the surface and then moves away.

To achieve high performance, Schubauer and Spangenberg (1960)[1] suggested a blade height of $h_v = 1.2\,\delta$. Thus, the height of the vortex line over the surface is assumed to be that of the boundary-layer outer edge, i.e., $h \approx \delta$ in this analysis, so that a more effective vortex flow to alleviate the flow separation may be expected. However, in order to correlate the geometric and position parameters affected by strong mixing, a larger value of h is also used for the computation. The origin of such a vortex line is assumed to be the midpoint of chord c_v. Since a three-dimensional vortex generator flow field is complex and deals with turbulent flow, no exact analytical solutions are expected. Hence, for convenience, it is assumed that the direction of the tip vortex line downstream of the generator is the same as the undistrubed flow direction; the neighboring vortex does not influence the vortex path, and the vortex does not burst. Comparative studies of the extent of the flow separation allieviation in terms of D/d, D/h, c_v/h, location of generators, and without a vortex generator are carried out so that the optimum conditions of separation alleviation may be determined. The coordinate systems of the vortex generator and the wing are shown in Figs. 3 and 4.

The induced velocity at an arbitrary point x,y,z due to tip vortex line A is given by Biot-Savart law as

$$(V_i)_A = \frac{\Gamma}{4\pi\sqrt{(y-h)^2+(z-d/2)^2}}\left[1 + \frac{x-x_v}{\sqrt{(x-x_v)^2+(y-h)^2+(z-d/2)^2}}\right] \qquad (1)$$

where x_v = vortex origin location,
h = tip vortex core height as well as tip vortex stream line height,
d = distance between two neighboring counter-rotating vortex lines,
Γ = vortex strength and its clockwise direction (positive when viewed from front to back).

The induced velocity in the z-direction is

$$(V_i)_{AZ} = \frac{\Gamma(h-y)}{4\pi[(y-h)^2+(z-d/2)^2]}\left[1 + \frac{x-x_v}{\sqrt{(x-x_v)^2+(y-h)^2+(z-d/2)^2}}\right]. \qquad (2)$$

Then the induced velocity in the z-direction due to tip vortex line A,B,C,D becomes

$$W_{ABCD} = \frac{\Gamma}{4\pi}\left\{\frac{h-y}{(y-h)^2+(z-d/2)^2}\left[1+\frac{x-x_v}{\sqrt{(x-x_v)^2+(y-h)^2+(z-d/2)^2}}\right]\right.$$
$$-\frac{h-y}{(y-h)^2+(z-d/2)^2}\left[1+\frac{x-x_v}{\sqrt{(x-x_v)^2+(y-h)^2+(z+d/2)^2}}\right]$$
$$-\frac{(h+y)}{(y+h)^2+(z+d/2)^2}\left[1+\frac{x-x_v}{\sqrt{(x-x_v)^2+(y+h)^2+(z+d/2)^2}}\right]$$
$$\left.+\frac{(h+y)}{(y+h)^2+(z-d/2)^2}\left[1+\frac{x-x_v}{\sqrt{(x-x_v)^2+(y+h)^2+(z-d/2)^2}}\right]\right\}. \quad (3)$$

Thus, the induced velocity in the z-direction due to the vortices shown in Fig. 3 is

$$W = \frac{\Gamma}{4\pi}\sum_{k=-\infty}^{\infty}\left(\frac{h-y}{(y-h)^2+[z-(kD+d/2)]^2}\left\{1+\frac{x-x_v}{\sqrt{(x-x_v)^2+(y-h)^2+[z-(kD+d/2)]^2}}\right\}\right.$$
$$-\frac{h-y}{(y-h)^2+[z-(kD-d/2)]^2}\left\{1+\frac{x-x_v}{\sqrt{(x-x_v)^2+(y-h)^2+[z-(kD-d/2)]^2}}\right\}$$
$$-\frac{h+y}{(y+h)^2+[z-(kD-d/2)]^2}\left\{1+\frac{x-x_v}{\sqrt{(x-x_v)^2+(y+h)^2+[z-(kD-d/2)]^2}}\right\}$$
$$\left.+\frac{h+y}{(y+h)^2+[z-(kD+d/2)]^2}\left\{1+\frac{x-x_v}{\sqrt{(x-x_v)^2+(y+h)^2+[z-(kD+d/2)]^2}}\right\}\right). \quad (4)$$

The complexity of the generator flow field and the low aspect ratio of the blade make accurate evaluation of Γ a formidable task. Thus Γ is evaluated using the Jones (1957)[3] approximate solution of strength Γ based on the lifting line theory; see Appendix A. For a given x and z,

$$\Gamma \approx \frac{a_v\, h\, U_v\, AR_v}{\frac{1}{\pi} + AR_v \int_0^h \frac{W}{\Gamma}\, dy}$$

where $AR_c = c_v/h$.

$\int_0^h \frac{W}{\Gamma} dy$ may be evaluated using Eq. 4.

BOUNDARY-LAYER FLOW ANALYSIS

If the boundary layer is thin and the Reynolds number is large, the steady three-dimensional boundary-layer equations for turbulent incompressible flow may be used. With the coordinate system shown in Fig. 4 these equations, taken from Nash and Patel (1972),[12] are as follows:

THREE-DIMENSIONAL WORKING EQUATIONS

Continuity:

$$\frac{\partial u}{h_x \partial x} + \frac{\partial v}{\partial y} + \frac{\partial w}{\partial z} = 0 \tag{5}$$

Momentum:

$$\frac{u}{h_x}\frac{\partial u}{\partial x} + v\frac{\partial u}{\partial y} + w\frac{\partial u}{\partial z} + \frac{1}{h_x}\frac{\partial}{\partial x}\left(\frac{p}{\varrho}\right) + \frac{\partial}{\partial y}\overline{u'v'} - \nu\frac{\partial^2 u}{\partial y^2} = 0 \tag{6}$$

$$\frac{\partial}{\partial y}\left(\frac{p}{\varrho}\right) = 0 \tag{7}$$

$$\frac{u}{h_x}\frac{\partial w}{\partial x} + v\frac{\partial w}{\partial y} + w\frac{\partial w}{\partial z} + \frac{\partial}{\partial z}\left(\frac{p}{\varrho}\right) + \frac{\partial}{\partial y}\overline{v'w'} - \nu\frac{\partial^2 w}{\partial y^2} = 0 \tag{8}$$

The scale factors $h_x = h_x(y)$, $h_y = 1$ and $h_z = 1$ were used in these equations.

According to Eq. 7, the pressure distribution is a function of x and z only, and the distribution may be determined from conditions at the edge of the boundary layer. Thus, Eqs. 6 and 8 yield

$$-\frac{1}{h_x}\frac{\partial}{\partial x}\left(\frac{p}{\varrho}\right) = \frac{U}{h_x}\frac{\partial U}{\partial x} + W\frac{\partial U}{\partial z} \text{ and} \tag{9}$$

$$-\frac{\partial}{\partial z}\left(\frac{p}{\varrho}\right) = \frac{U}{h_x}\frac{\partial W}{\partial x} + W\frac{\partial W}{\partial z}. \tag{10}$$

For solutions to the boundary-layer equations, the Reynolds stresses are evaluated using the Boussinesq eddy viscosity hypothesis

$$-u'v' = \varepsilon\frac{\partial u}{\partial y}, \quad -v'w' = \varepsilon\frac{\partial w}{\partial y}. \tag{11}$$

Substituting into Eqs. 5, 6, and 8, the equations are nondimensionalized by letting

$$\bar{x} = \frac{x}{c} , \bar{y} = \frac{y}{c} \left(\frac{U_\infty c}{\nu}\right)^{1/2} , \bar{z} = \frac{z}{c}$$

$$\bar{u} = \frac{u}{U_\infty} , \bar{v} = \frac{v}{U_\infty} \left(\frac{U_\infty c}{\nu}\right)^{1/2} , \bar{w} = \frac{w}{U_\infty}$$

$$\bar{p} = \frac{p}{\varrho U_\infty^2} , \bar{\varepsilon} = \frac{\varepsilon}{\nu}$$

where c is the chord length of the airfoil.

The working equations become

$$\frac{1}{h_x} \frac{\partial \bar{u}}{\partial x} + \frac{\partial \bar{v}}{\partial y} + \frac{\partial \bar{w}}{\partial z} = 0 \tag{12}$$

$$\frac{\bar{u}}{h_x} \frac{\partial \bar{u}}{\partial \bar{x}} + \bar{v} \frac{\partial \bar{u}}{\partial \bar{y}} + \bar{w} \frac{\partial \bar{u}}{\partial \bar{z}} = - \frac{\partial \bar{p}}{h_x \partial \bar{x}} + \frac{\partial}{\partial \bar{y}} \left[(1+\bar{\varepsilon}) \frac{\partial \bar{u}}{\partial \bar{y}}\right] \tag{13}$$

$$\frac{\bar{u}}{h_x} \frac{\partial \bar{w}}{\partial \bar{x}} + \bar{v} \frac{\partial \bar{w}}{\partial \bar{y}} + \bar{w} \frac{\partial \bar{w}}{\partial \bar{z}} = - \frac{\partial \bar{p}}{\partial \bar{z}} + \frac{\partial}{\partial \bar{y}} \left[(1+\bar{\varepsilon}) \frac{\partial \bar{w}}{\partial \bar{y}}\right] . \tag{14}$$

For convenience, superscript $^-$ is dropped from these equations. In the vortex generator flow field, U_∞ is replaced by U_v, and coordinates x,y,z are defined accordingly in this region (Fig. 3).

On the plane of symmetry, w = 0; thus Eq. (14) can be eliminated. However, for the solution, the number of equations is not sufficient compared to the unknowns, and an additional equation is derived by differentiating Eq. (14) with respect to z,

$$\frac{u}{h_x} \frac{\partial w_z}{\partial x} + v \frac{\partial w_z}{\partial y} + w_z^2 = - \frac{\partial^2}{\partial z^2} \left(\frac{p}{\varrho}\right) + \frac{\partial}{\partial y} \left[(1+\varepsilon) \frac{\partial w_z}{\partial y}\right] \tag{15}$$

where $w_z = \frac{\partial w}{\partial z}$.

At the edge of the boundary layer, Eq. 15 reduces further to

$$- \frac{\partial^2}{\partial z^2} \left(\frac{p}{\varrho}\right) = \frac{U}{h_x} \frac{\partial W_z}{\partial x} + W_z^2 . \tag{16}$$

The boundary-layer displacement and momentum thicknesses in streamline directions are defined, as

for $u_s = u \cos \beta + w \sin \beta$, $\left(\beta = \tan^{-1} \frac{W}{U}\right)$,

$$\text{as } \delta^* = \int_0^\infty \left(1 - \frac{u_s}{U_s}\right) dy , \theta = \int_0^\infty \left(1 - \frac{u_s}{U_s}\right)\left(\frac{u_s}{U_s}\right) dy, \text{ and } H = \frac{\delta^*}{\theta} . \tag{17}$$

The flow on the wing influenced by all the vortex generators is analyzed in a small computational domain of the wing span. The vortex generators are located upstream of the normal flow separation line for the clean-surface airfoil.

The computation of flow characteristics starts from the forward stagnation point. The upstream laminar flow is assumed to be tripped by insect or rain contamination and becomes turbulent very early at $Re_\theta = 320$. For the purpose of assessing the extent of the flow separation alleviation, the separation region has been defined as that downstream of the locations where $C_{f_x} = 0$.

The laminar, transition, and turbulent flow regimes are included in the computations. The extent of the transition region is considered in the computations by multiplying the eddy viscosity by the intermittency factor γ_{tr} defined by Chen and Thyson (1971)[13] and by Cebeci and Smith (1974).[14]

$$\gamma_{tr} = 1 - \exp\left[-G\,(x - x_{tr}) \int_{x_{tr}}^{x} \frac{dx}{U_s}\right]$$

where G is the spot formation parameter defined by

$$G = \frac{3}{c^2}\left(\frac{U_s^3}{\nu^2}\right) R_{ex_{tr}}^{-1.34}$$

and

$$c = 60 + 4.86\, M_s^{1.92}, \qquad 0 < M_s < 5$$

(for incompressible flow c = 60).

An effort to find a suitable eddy viscosity model applicable to the expected strong mixing of outer and inner flow regions due to the streamwise vortices was not successful. Thus, the algebraic turbulence model of Cebeci and Smith (1974)[14] and its extension was selected for its simplicity and modest computer resource demands. The model is described in Appendix B.

BOUNDARY AND INITIAL CONDITIONS

For the computation, it is assumed that the vortex line downstream of the vortex generator is parallel to the U-direction and that the vortex does not influence the U-velocity.

The boundary conditions are

at $y = 0$, $u = v = w = w_z = 0$;

at $y = \delta$, $u = U$, $w = W$, $w_z = W_z$;

at $z = 0$ and on the plane of symmetry,

$$w = W = 0, \frac{\partial u}{\partial z} = \frac{\partial v}{\partial z} = 0.$$

The initial conditions of flow are determined at the forward stagnation region of wing leading edge using Hiemenz's stagnation flow solutions (Schlichting 1960,[15] pp. 79-83), as

$$\frac{w}{W} \approx \frac{u}{U} \text{ (Chang and Patel, 1975).}^{16}$$

FINITE DIFFERENCE FORMULATION

The Crank-Nicolson finite difference method is applied with the grid structures (Fig. 5) to solve the continuity and momentum equations of the three-dimensional turbulent boundary-layer flow.

FORMULATION AND ATTACHED FLOW GRID STRUCTURE

Any variables V and their derivatives are approximately given by the following equations (Chang and Patel, 1975)[16] derived from Klinksiek and Pierce (1973):[17]

$$V = \frac{1}{4}\left[V(i+1,j,k) + V(i,j,k) + V(i+1,j,k-1) + V(i,j,k-1)\right] \tag{18}$$

$$\frac{\partial V}{\partial x} = \frac{1}{2\Delta x}\left[V(i+1,j,k) - V(i,j,k) + V(i+1,j,k-1) - V(i,j,k-1)\right] \tag{19}$$

$$\frac{\partial V}{\partial z} = \frac{1}{2\Delta z}\left[V(i+1,j,k) - V(i+1,j,k-1) + V(i,j,k) - V(i,j,k-1)\right] \tag{20}$$

$$\begin{aligned}\frac{\partial V}{\partial y} = \frac{1}{4(\Delta y_+ + \Delta y_-)}\Bigg\{\frac{\Delta y_-}{\Delta y_+}\Big[&V(i,j+1,k) - V(i,j,k)\\ &+ V(i,j+1,k-1) - V(i,j,k-1) + V(i+1,j+1,k)\\ &- V(i+1,j,k) + V(i+1,j+1,k-1) - V(i,j,k-1)\Big]\\ + \frac{\Delta y_+}{\Delta y_-}\Big[&V(i,j,k) - V(i,j-1,k) + V(i,j,k-1)\\ &- V(i,j-1,k-1) + V(i+1,j,k) - V(i+1,j-1,k)\\ &+ V(i+1,j,k-1) - V(i+1,j-1,k-1)\Big]\Bigg\}\end{aligned} \tag{21}$$

$$\begin{aligned}\frac{\partial}{\partial y}\left[(1+\varepsilon)\frac{\partial V}{\partial y}\right] = \frac{1}{2(\Delta y_+ + \Delta y_-)}\Bigg\{&[1+\varepsilon(i+1,j+1/2,k)]\frac{V(i+1,j+1,k)-V(i+1,j,k)}{\Delta y_+}\\ &- [1+\varepsilon(i+1,j-1/2,k)]\frac{V(i+1,j,k)-V(i+1,j-1,k)}{\Delta y_-}\\ &+ [1+\varepsilon(i+1,j+1/2,k-1)]\frac{V(i+1,j+1,k-1)-V(i+1,j,k-1)}{\Delta y_+}\end{aligned}$$

$$- [1+\varepsilon(i+1,j-1/2,k-1)] \frac{V(i+1,j,k-1)-V(i+1,j-1,k-1)}{\Delta y_-}$$

$$+ [1+\varepsilon(i,j+1/2,k)] \frac{V(i,j+1,k)-V(i,j,k)}{\Delta y_+}$$

$$- [1+\varepsilon(i,j-1/2,k)] \frac{V(i,j,k)-V(i,j-1,k)}{\Delta y_-}$$

$$+ [1+\varepsilon(i,j+1/2,k-1)] \frac{V(i,j+1,k-1)-V(i,j,k-1)}{\Delta y_+}$$

$$- [1+\varepsilon(i,j-1/2,k-1)] \frac{V(i,j,k-1)-V(i,j-1,k-1)}{\Delta y_-} \Bigg\}. \qquad (22)$$

If Δx, Δz, Δy_+ and Δy_- are formulated by

$$\Delta x = x(i+1)-x(i),\ \Delta z = z(k)-z(k-1)$$

$$\Delta y_+ = y(j+1)-y(j),\ \Delta y_- = y(j)-y(j-1),$$

then the momentum Eqs. 13 and 14 can be arranged as a tri-diagonal matrix.

$$A(j)\ u(i+1,j-1,k) + B1(j)\ u(i+1,j,k) + C(j)\ u(i+1,j+1,k) = D1(j) \qquad (23)$$

$$A(j)\ w(i+1,j-1,k) + B2(j)\ w(i+1,j,k) + C(j)\ w(i+1,j+1,k) = D2(j) \qquad (24)$$

Coefficients A(j), C(j), B1(j), B2(j), B3(j) are described in Appendix C.

On the symmetric plane, from Eqs. 13 and 15,

$$A(j)\ u(i+1,j-1,k) + B3(j)\ u(i+1,j,k) + C(j)\ u(i+1,j+1,k) = D3(j) \qquad (25)$$

$$A(j)\ w_z(i+1,j-1,k) + B4(j)\ w_z(i+1,j,k) + C(j)\ w_z(i+1,j+1,k) = D4(j). \qquad (26)$$

These tri-diagonal matrices are solved by the Thomas algorithm.

The velocity component v in the y-direction is determined using the continuity equation and applying the backward-difference formula given by

$$v(i+1,j,k) = v(i+1,j-1,k)$$

$$- \frac{\Delta y_j}{2} \Bigg\{ \frac{1}{h_x \Delta x} [u(i+1,j,k) - u(i,j,k)$$

$$+ u(i+1,j-1,k) - u(i,j-1,k)]$$

$$- \frac{1}{\Delta z} [w(i+1,j,k) - w(i+1,j,k-1)$$

$$+ w(i+1,j-1,k) - w(i+1,j-1,k-1)]\Big\} \tag{27}$$

$$\Delta y_j = y(j) - y(j-1) \qquad j = 2, 3 \ldots n+1.$$

This equation is used for the grid shown in Fig. 5 for the solution of attached flow.

GRID STRUCTURE FOR SEPARATED FLOW

For the separated flow, as shown in the grid structure (Fig. 6), terms for the $(i+1,j,k-1)$ points in the region of the separated flow region are excluded. Thus, for the momentum equation solution,

$$V = \frac{1}{2}[V(i+1,j,k) + V(i,j,k)] \tag{28}$$

$$\frac{\partial v}{\partial x} = \frac{1}{\Delta x}[V(i+1,j,k) - V(i,j,k)] \tag{29}$$

$$\frac{\partial v}{\partial z} = \frac{1}{\Delta z}[V(i+1,j,k) - V(i,j,k)] \tag{30}$$

$$\frac{\partial v}{\partial y} = \frac{1}{2(\Delta y_+ + \Delta y_-)}\Big\{\frac{\Delta y_-}{\Delta y_+}[V(i,j+1,k) - V(i,j,k) + V(i,j+1,k) - V(i+1,j,k)] + \frac{\Delta y_+}{\Delta y_-}[V(i,j,k) - V(i,j-1,k) + V(i+1,j,k) - V(i+1,j-1,k)]\Big\} \tag{31}$$

and for the continuity equation solution,

$$\frac{\partial u}{\partial x} = \frac{1}{2\Delta x}[u(i+1,j,k) - u(i,j,k) + u(i+1,j-1,k) - u(i,j-1,k)] \tag{32}$$

$$\frac{\partial v}{\partial y} = \frac{1}{2\Delta y_-}[v(i+1,j,k) - v(i+1,j-1,k) + v(i,j,k) - v(i,j-1,k)] \tag{33}$$

$$\frac{\partial w}{\partial z} = \frac{1}{2\Delta z}[w(i,j,k) - w(i,j,k-1) + w(i,j-1,k) - w(i,j-1,k-1)]. \tag{34}$$

The local grid spacings used across the boundary-layer thickness are

a. For laminar flow

$$y_{j+1} = \delta_{max}\left[C_m \frac{j}{n} + (1-C_m)\left(\frac{j}{n}\right)^2\right], \qquad j=1, 2, \ldots, n. \tag{35}$$

Because the velocity changes rapidly close to the wall, grid size is made small by taking $C_m < 1$. Boundary-layer thickness is evaluated by the minimum grid height satisfying

$$\left| \left[\frac{u^2(i,n,k) + w^2(i,n,k)}{U^2 + W^2} \right]^{1/2} - 1 \right| < 0.0005. \tag{36}$$

For $C_m = 1$, the grid spacing is uniform.

b. For turbulent flow.

Following Cebeci and Smith (1974),[14] the grid spacing in the y direction is specified using a geometric progression with the ratio of any two adjacent intervals being a constant. Thus,

$$\Delta y_{j+1} = \gamma \Delta y_j \tag{37}$$

$$y_{j+1} = \Delta y_2 \frac{\gamma^j - 1}{\gamma - 1} \qquad \gamma > 1, \tag{38}$$

$$n+1 = \frac{\ell n[1 + (\gamma - 1)\delta max/\Delta y_2]}{\ell n\, \gamma} \tag{39}$$

where $\Delta y_2 = y_2 - y_1$. This technique allows many grid points close to the wall and holds the total points across the boundary layer to a reasonable number. Since the grid in the area of the surface must be smaller than in the viscous sublayer, the initial spacing was taken by satisfying $\Delta y_2 u^*/\nu < 4$. The turbulent boundary-layer thickness was evaluated as in the case of laminar flow, using Eq. 36. The total number of points in the y direction was in the range of n = 24 to 35. The step size in the x-direction is proportional to the boundary-layer thickness (typically $\Delta x \approx \delta$). The step size in the z-direction is held constant (typically $\Delta z \approx 0.025D$).

RESULTS AND DISCUSSIONS

Numerical computations are carried out for the vortex generator turbulent flow on a thick airfoil section. The airfoil and velocity distributions were generated using Schopper's (1983)[18] airfoil design computer program which is based on Lighthill's (1945)[19] inverse method. The airfoil and velocity distribution are shown in Fig. 7.

Since such a thick wing may be useful for a high lift-to-drag ratio, low-speed cargo plane, the numerical evaluations are performed for a cruising speed of 130 ft/s and a 10-ft chord length ($Re_c = 8 \times 10^7$ and $s_u = 12.5$ ft). The angle of attack is 8 deg (lift coefficient = 1.03). The distributions of boundary-layer shape factor H and skin friction coeficient C_f are shown in Fig. 8 for a smooth airfoil. As indicated by the rapid increase of H as well as by the rapid decrease of C_f approaching the separation point, the flow without vortex generators separates at $x/s_u = 0.82$, where s_u is the upper surface length of the airfoil. The separation point is located at the position where $C_{f_x} = 0$ and H = 2.36. The separation region is illustrated in Figs. 9, 10, and 11.

Figure 9 presents an overview of the y = 0 plane showing the vortex generators, the separation region, and the computational domain of the vortex generator flow. As shown in Fig. 9, the separation line downstream of the vortex generator is curved. Such non-straight-line behavior of the separation line was also observed by Schubauer and Spangenberg (1960).[1]

The extent of the flow separation alleviation due to the vortex generator can be assessed by comparing the separation line of the vortex generator flow shown in Figs. 10 and 11 with the flow separation line without the vortex generators. The vortex generator flow separation line is affected by the position, size, and arrangement of the vortex generators, i.e., by x_v, D, d, c_v, h, α_v, etc. Since these factors are numerous and flow interaction may take place, it is not an easy task to interpret the flow separation behavior. Nevertheless, an attempt was made to illustrate the separation behavior by choosing parameters D/h and D/d and by determining the geometrically feasible values of c_v/h so that no blade crossing would occur. Determination of such c_v/h values is described in Appendix D.

Examples of the separation lines are shown in Figs. 10 through 13 for the following range of parameters: α_v = 15 deg, h = 0.15 ft and 0.5 ft, D/h = 2-5 and 10, D/d = 2-4, and c_v/h = 1.25 to 8.

One example of the investigations of effectiveness of separation alleviation as a function of vortex generator location is shown in Fig. 10. For these computations h was fixed at 0.15 ft, and the values of D/h and c_v/h were taken as 10 and 1.25, respectively. Since good generator performance can be obtained with a blade height of $h_v \sim 1.2\delta$, computations of δ along s_u indicate that, for generator locations of x_v/s_u = 0.4 through 0.7, the fixed generator height value may serve to allow assessment of the effect of generator location on generator performance. As shown in Fig. 10, the separation line is located farther downstream as the generator is moved upstream. The figure also shows that performance improves as the spanwise spacing, D/d, increases.

Figure 11 presents separation line results for the generator fixed at x_v/s_u = 0.4 and various values of the parameters D/h, D/d, and c_v/h. For this study h = 0.5 ft is assumed, and although this value is larger than 1.2δ and the results are strongly affected by turbulence mixing, the value appears to be suitable to evaluate the correlation of geometric and position parameters. Figure 11 also shows that the separation point moves downstream along the symmetry axis A and moves upstream along the symmetry axis B ahead of the separation line which occurs without the vortex generator.

Wang (1970)[20] found that, for the three-dimensional boundary layer near the plane of symmetry of a spheroid at an angle of attack, at least near the symmetry plane, separation occurs upstream of the streamwise separation point defined by the location at which the surface streamlines from each side converge and meet tangentially. Wang conjectures that this phenomenon is attributable to the cross-flow separation (i.e., due to the reversal of v velocity). Further investigations of cross-flow separation of the vortex generator may clarify this phenomenon.

Since the extent of the upstream region of separation beyond the separation line without the vortex generator is small, the vortex generator is effective with larger c_v/h values, although the effectiveness does not increase much and remains nearly unchanged with values of $c_v/h > 6$. It should also be noted that, with equal values of

D/h and c_v/h, the separation region is reduced as D/d increases, indicating higher efficiency of separation alleviation with larger D/d.

Figure 12 presents shape factor distributions as a function of surface distance and parameters D/d, D/h, and z when the vortex generator is fixed at $x_v/s_u = 0.4$. Over most of the acceleration portion of the airfoil, $x/s_u \leq 0.55$, the shape factor is nearly constant at $H \sim 1.5$. In the airfoil deceleration region, the shape factors show earlier and steeper growth with increasing z, that is, with increasing distance from the symmetry axis A. Along the symmetry axis, the results are nearly independent of D/d, D/h, and z.

Figure 13 shows streamwise skin friction distribution when the generator is located at $x_v/s_u = 0.4$. Here C_{f_x} decreases rapidly in the deceleration region and reaches the value of zero at the separation point. With increase of z, separation occurs earlier. As seen in Fig. 13c, for D/h = 3 and 4 separation is completely suppressed up to the trailing edge.

Additional study of the computed results (not reported herein) may establish optimum conditions of the vortex generator flow to alleviate the flow separation. It would be of interest to investigate the extent of separation alleviation by installing a staggered double row of vortex generators. The analysis could be improved by applying the newest turbulence model of Cebeci et al. (1987)[21] for two-dimensional and three-dimensional turbulent flow involving flow separation. Since the vortex generators cause drag, a drag analysis of the vortex generator also would be of interest.

CONCLUSIONS

A numerical turbulent flow analysis of counter-rotating vortex generators attached to a large aspect ratio wing has been performed for the case of $Re_c = 8 \times 10^7$. The Cebeci et al. turbulence model has been used under the assumption that transition occurs near the leading edge at $Re_\theta = 320$. The following conclusions have been reached:

1. With an increase of c_v/h, the separation point moves downstream; along the symmetric axis of the vortex generator (z = 0). Along the symmetric axis between the vortex generators (z = D/2), the separation point is located a short distance upstream of the separation line without the vortex generator. Nevertheless, the effectiveness of the vortex generator in alleviating flow separation is evident. When c_v/h is large (greater than about 4), separation is completely suppressed in the axis region of the vortex generator. Beyond a certain limit, perhaps $c_v/h > 6$, the effectiveness of the vortex generator does not increase appreciably.
2. Separation is more effectively suppressed as the vortex generator is moved upstream and as the spacing between the pairs of counter-rotating vortices is increased.
3. The behavior of the distributions of H and C_{f_x} along the vortex generator symmetric axis is nearly identical for all cases of separated flow computed and is not affected by D/d, D/h, and c_v/h, but depends on the spanwise distance z. With a decrease in z, separation occurs later, and in some cases separation is prevented.

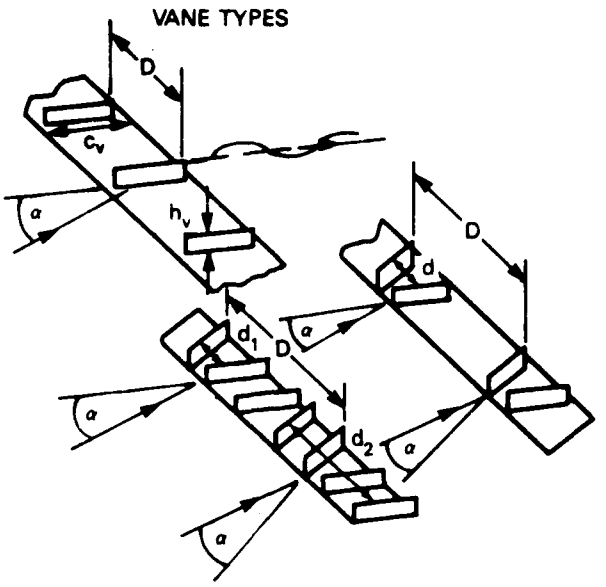

Fig. 1. Examples of vane-type vortex generators (Pearcey [1961][4]).

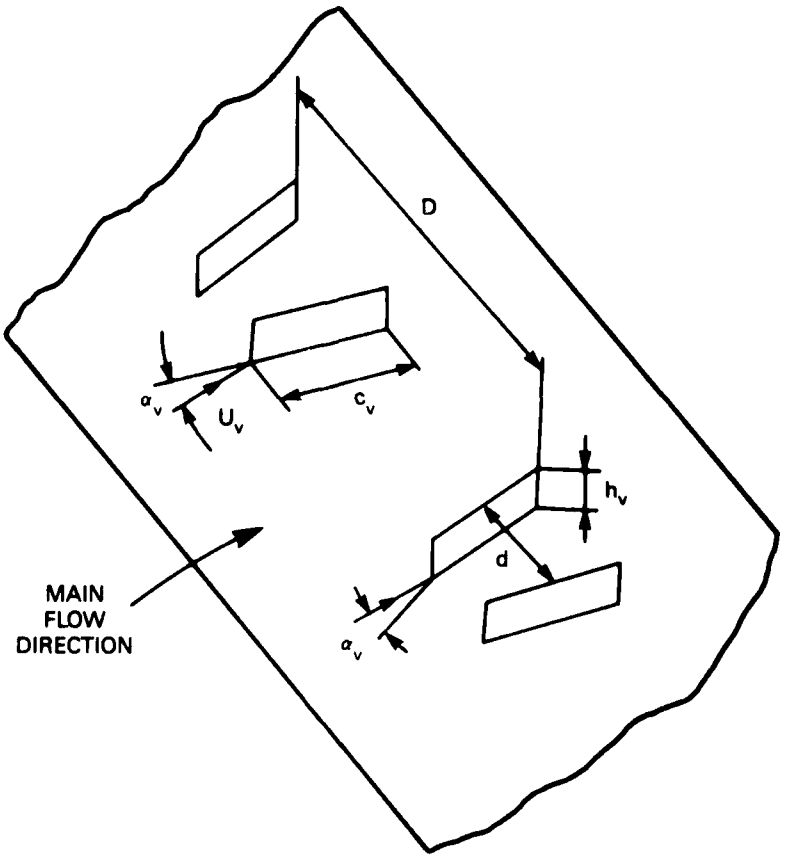

Fig. 2. Counter-rotating vane-type vortex generator.

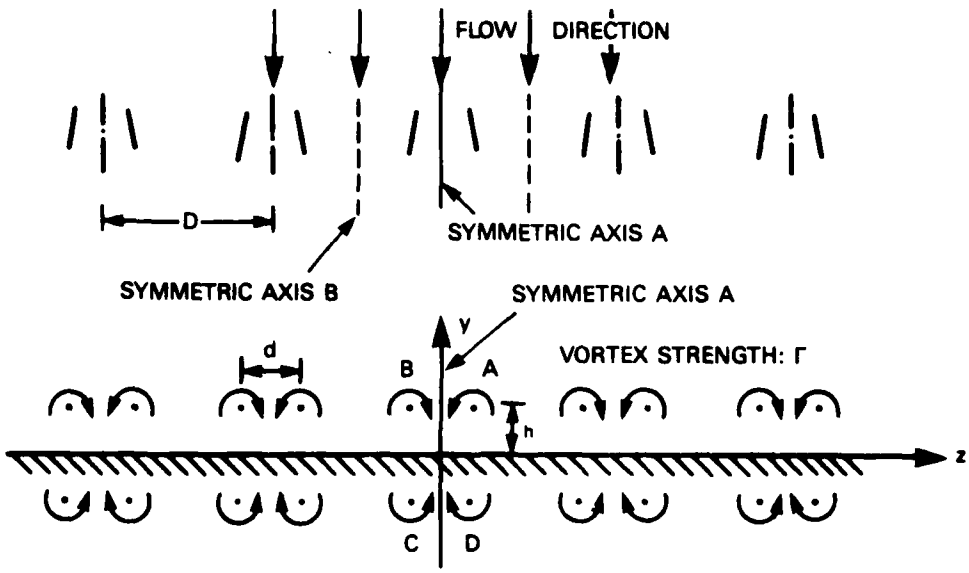

Fig. 3. Vortex generator arrangement.

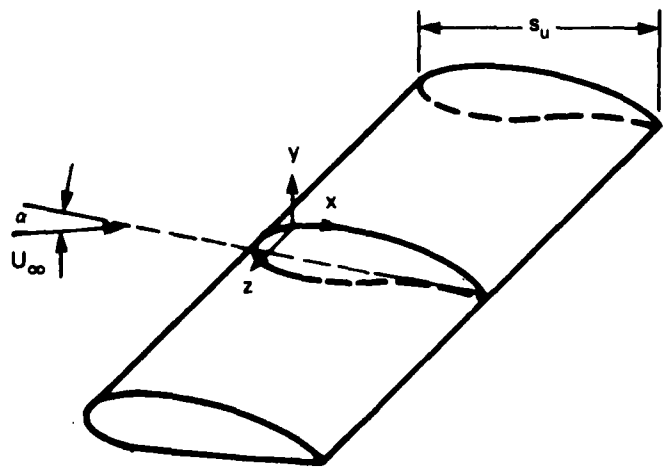

Fig. 4. Coordinate system.

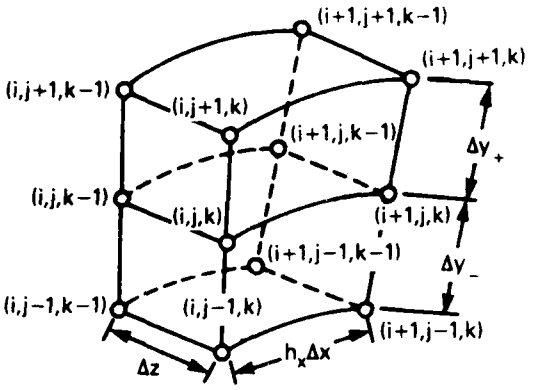

Fig. 5a. Grid for momentum equation.

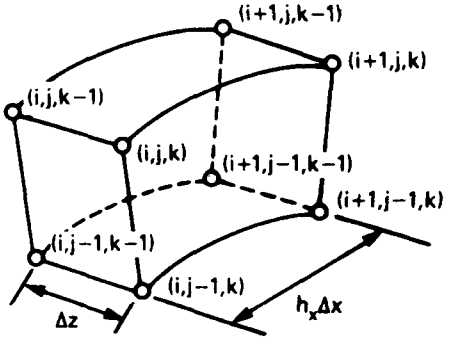

Fig. 5b. Grid for continuity equation.

Fig. 5. Grid structure.

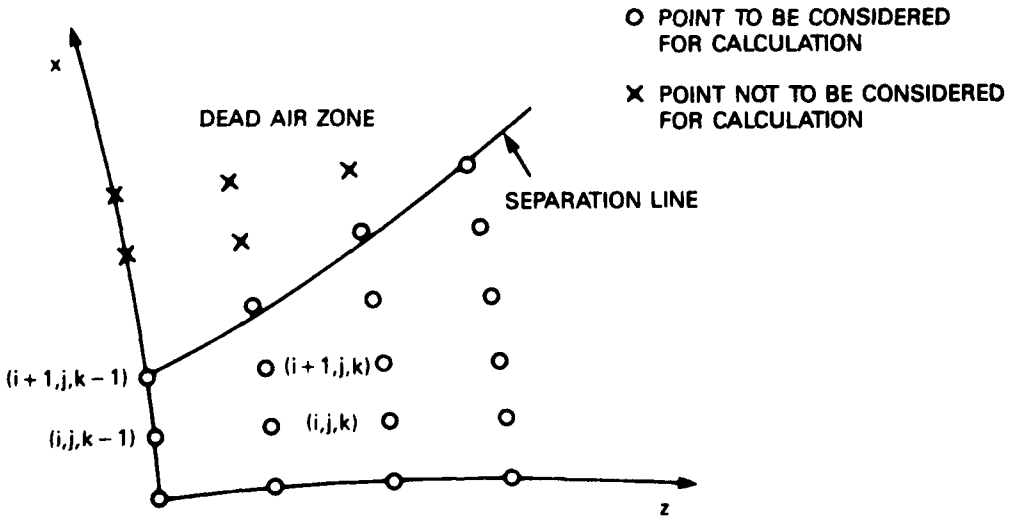

Fig. 6. Grid points for determination of separation line.

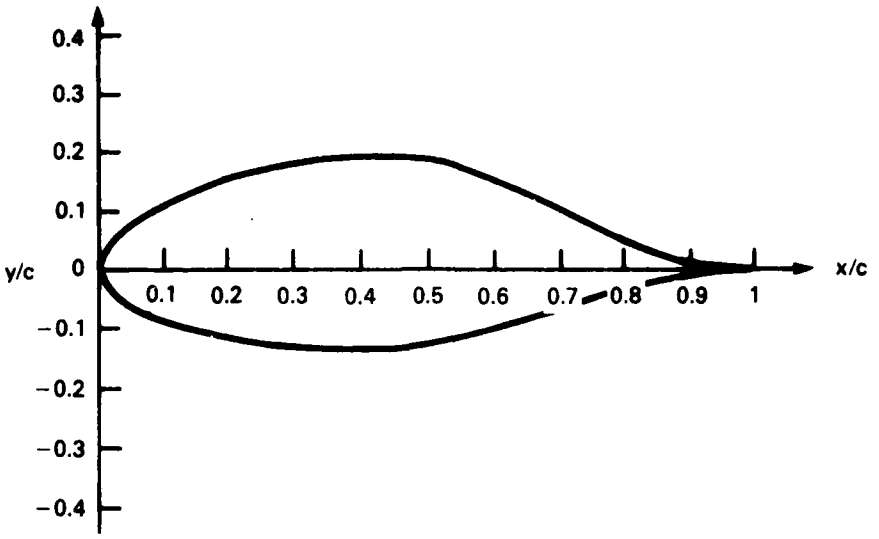

Fig. 7a. Airfoil configuration.

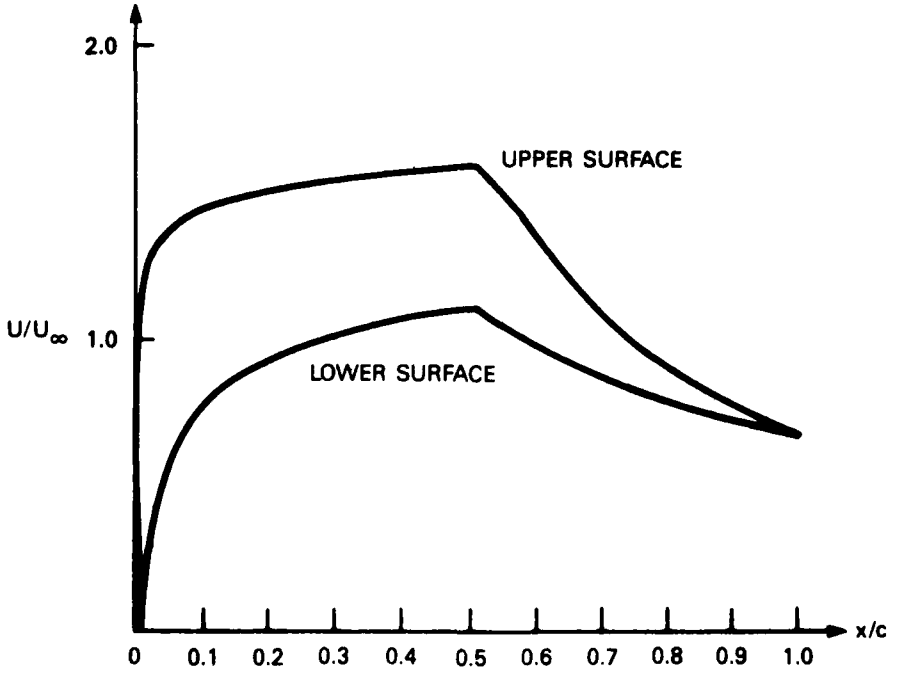

Fig. 7b. Velocity distribution on airfoil surface ($\alpha = 8°$).

Fig. 7. Sketch of configuration and velocity distribution of airfoil.

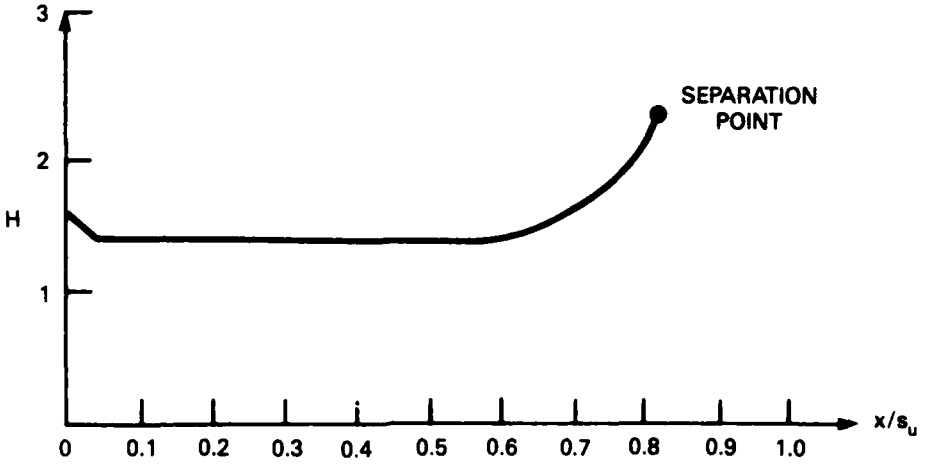

Fig. 8a. Shape factor H along main stream direction.

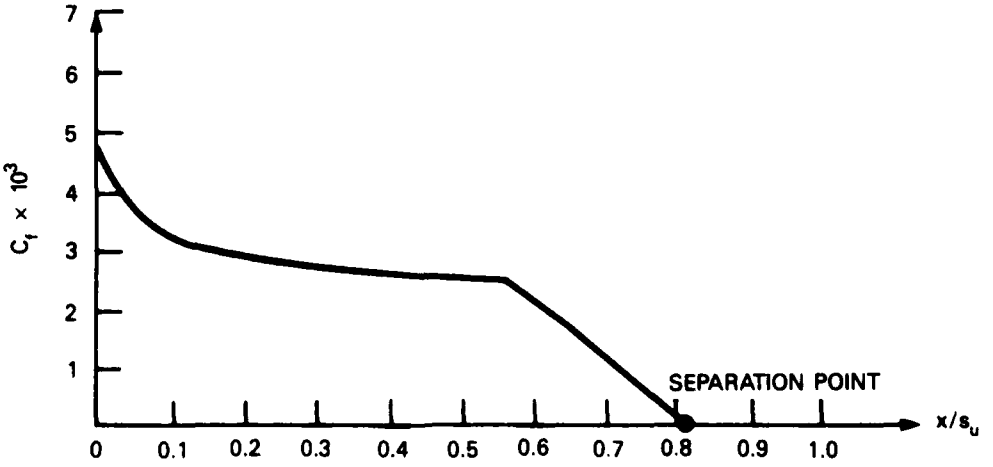

Fig. 8b. Skin friction coefficient C_f distribution.

Fig. 8. H and C_f behavior in absence of vortex generator ($\alpha = 8°$).

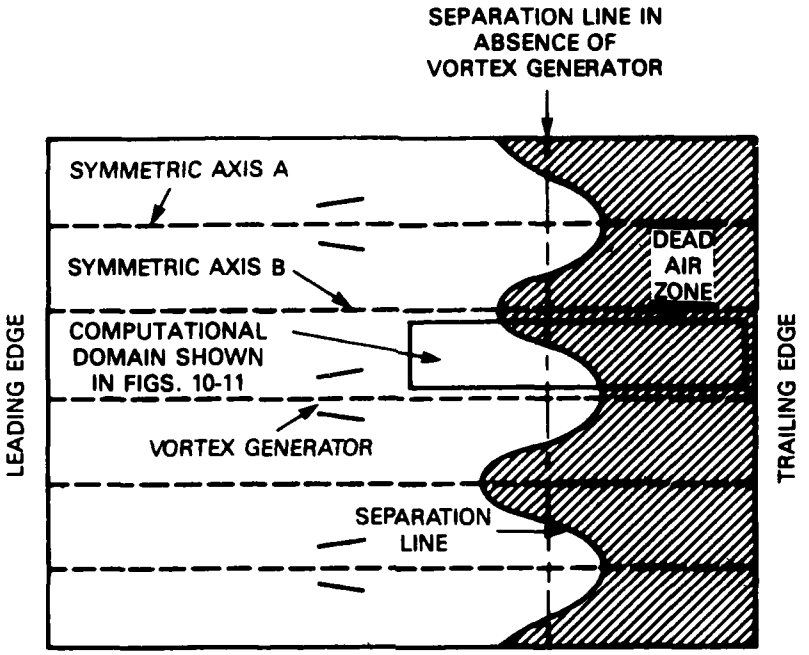

Fig. 9a. Separation line for weak alleviation.

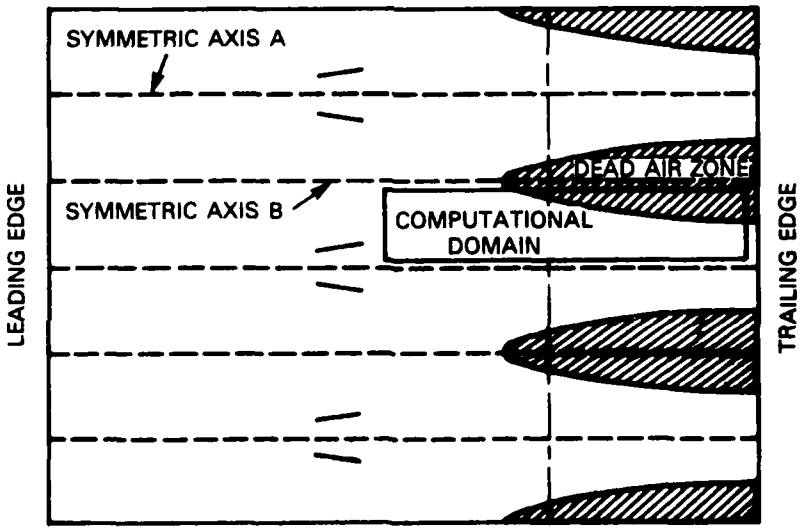

Fig. 9b. Separation line for strong alleviation.

Fig. 9. Sketch of separation line of vortex generator flow field (overview y = 0).

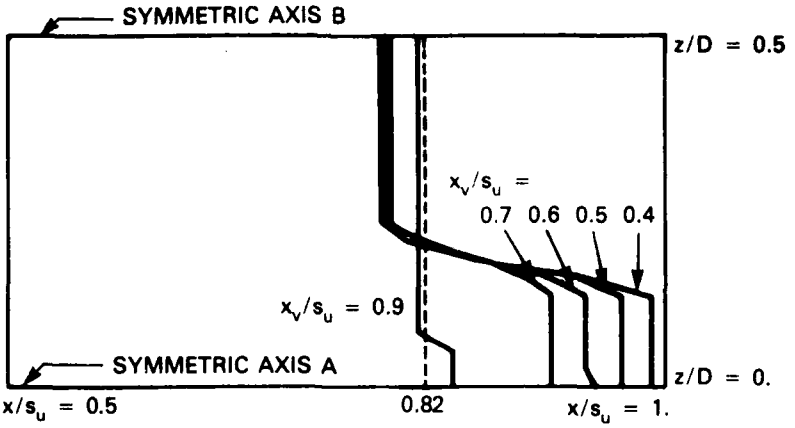

Fig. 10a. D/d = 4.

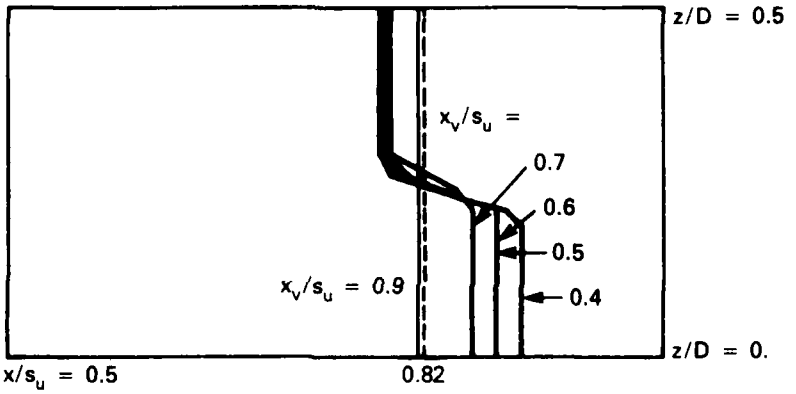

Fig. 10b. D/d = 3.

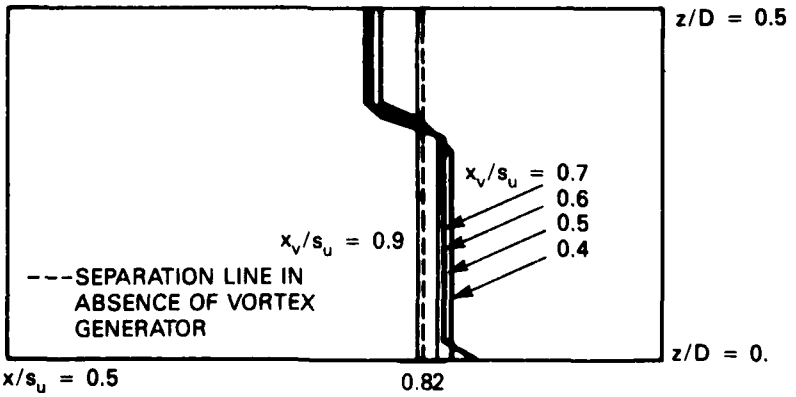

Fig. 10c. D/d = 2.

(h=0.15 ft, D/h=10, c_v/h=1.25, α_v=15°)

(z=0 — SYMMETRIC AXIS A, z/D=0.5 — SYMMETRIC AXIS B)

Fig. 10. Separation line in parameter of x_v/s_u.

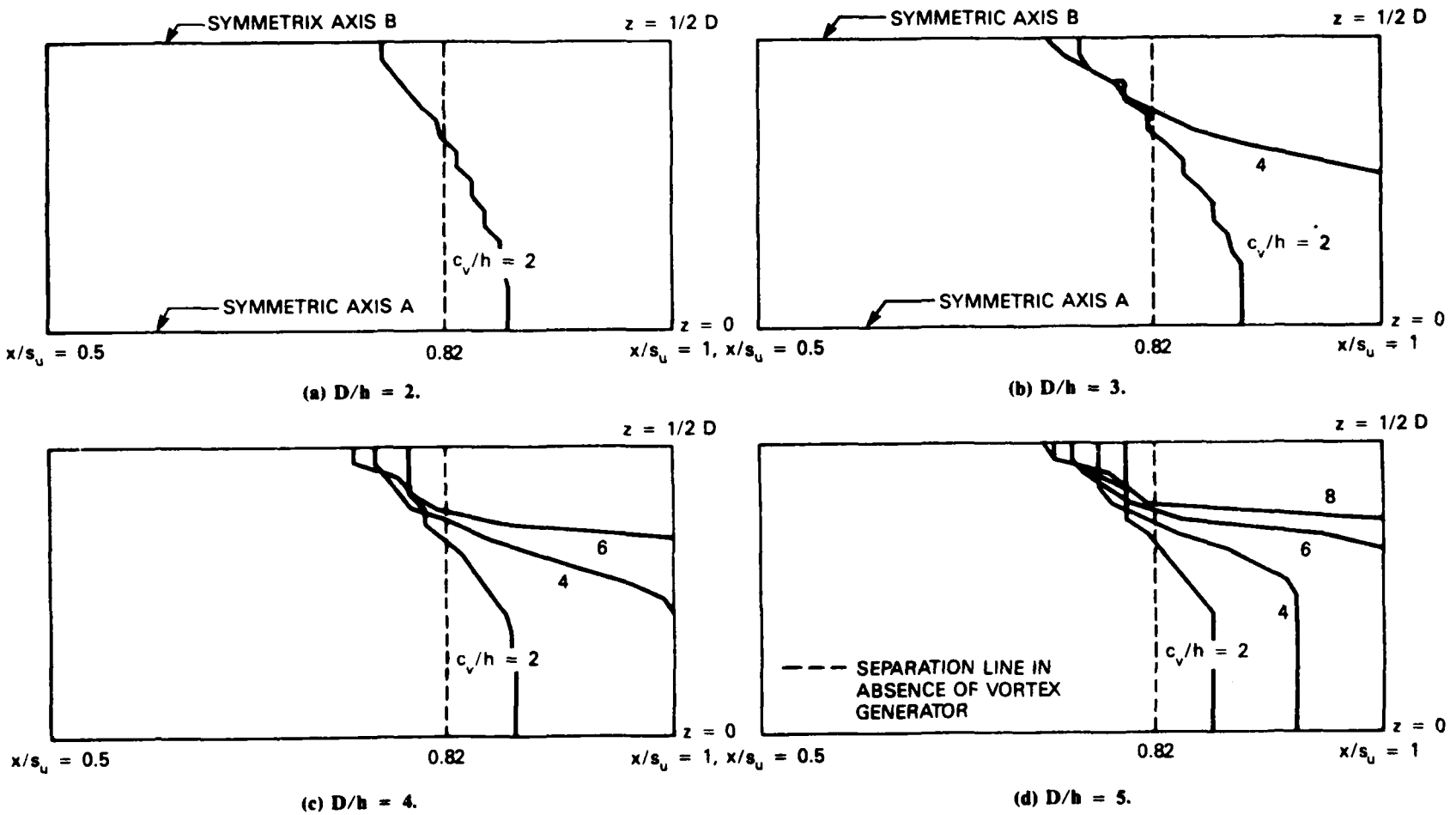

(a) D/h = 2.

(b) D/h = 3.

(c) D/h = 4.

(d) D/h = 5.

(x_v/s_u = 0.4, h = 0.5 ft, α_v = 15°
(z = 0 – SYMMETRIC AXIS A
z = 1/2 D – SYMMETRIC AXIS B)

Fig. 11a. D/d = 2.

Fig. 11. Separation line on y = 0 surface.

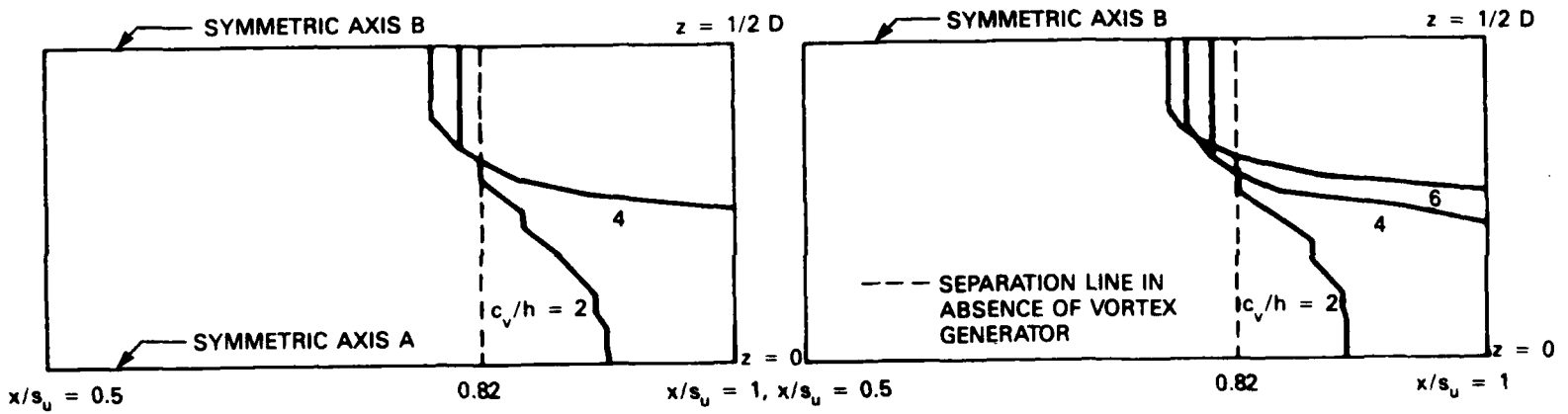

(a) D/h = 4.

(b) D/h = 5.

(x_v/s_u = 0.4, h = 0.5 ft, α_v = 15°
(z = 0 – SYMMETRIC AXIS A
z = 1/2 D – SYMMETRIC AXIS B)

Fig. 11b. D/d = 3.

Fig. 11. (Continued)

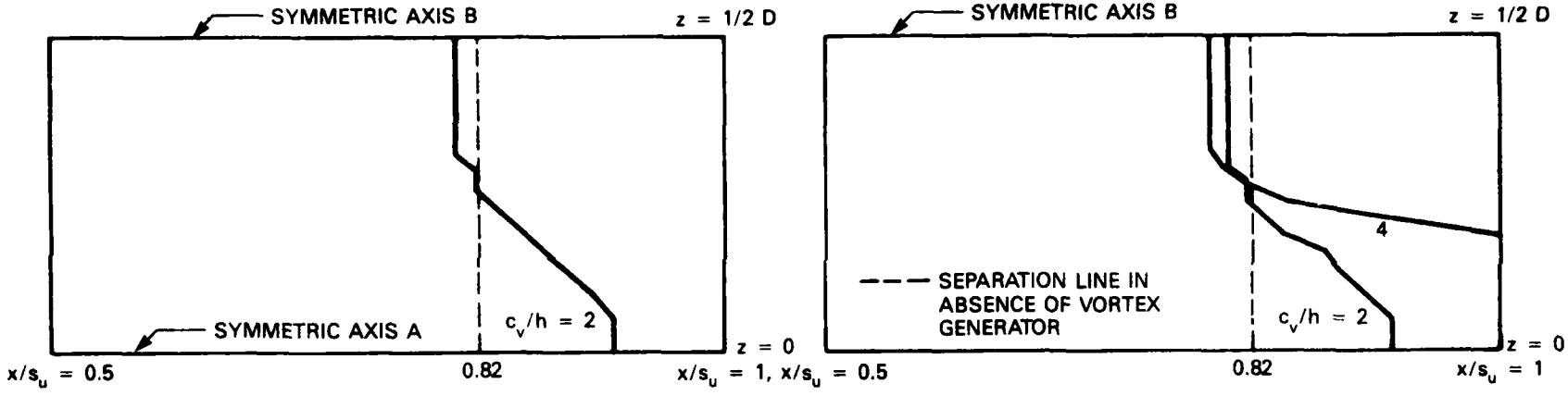

(a) D/h = 4.

(b) D/h = 5.

(x_v/s_u = 0.4, h = 0.5 ft, α_v = 15°
(z = 0 – SYMMETRIC AXIS A
z = 1/2 D – SYMMETRIC AXIS B)

Fig. 11c. D/d = 4.

Fig. 11. (Continued)

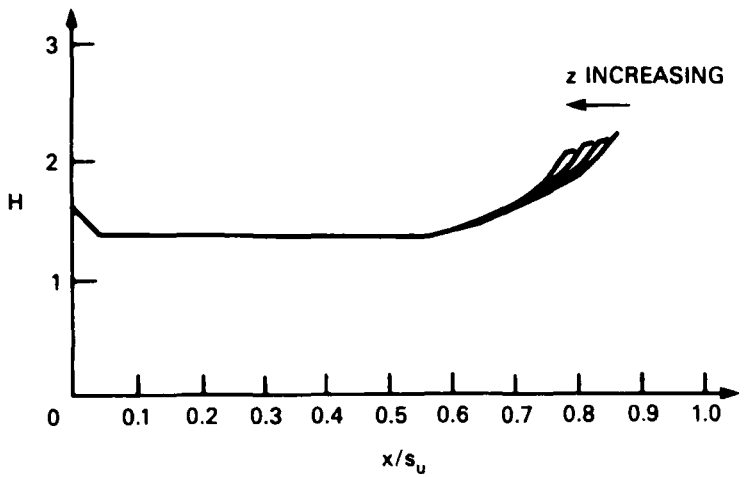

(a) D/h = 2.

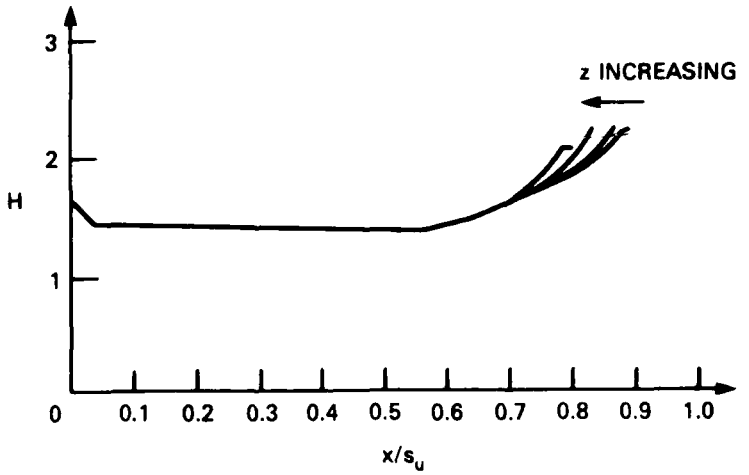

(b) D/h = 3.

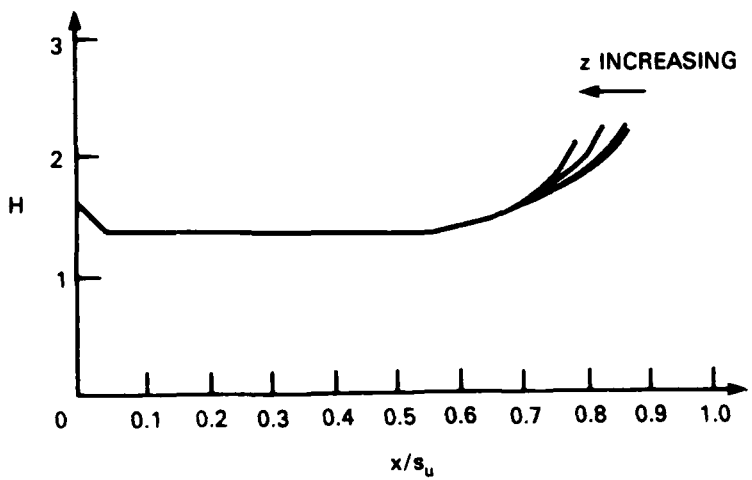

(c) D/h = 4.

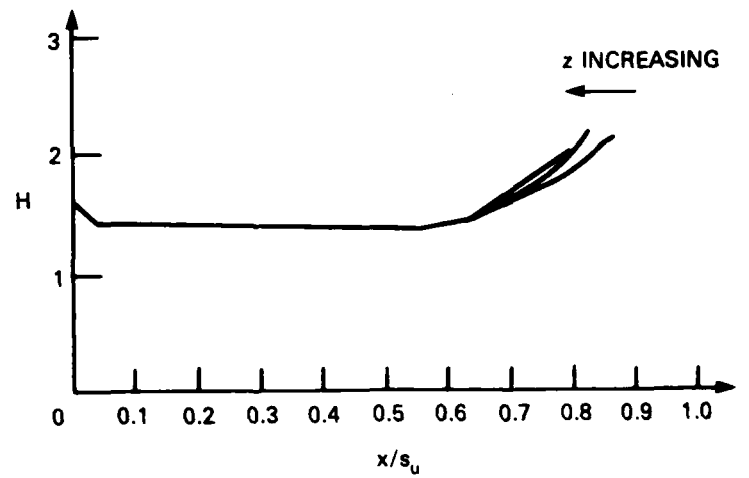

(d) D/h = 5.

(x_v/s_u = 0.4, h = 0.5 ft, α_v = 15°)

Fig. 12a. D/d = 2, c_v/h = 2.

Fig. 12. Shape factor H curve in parameter of z.

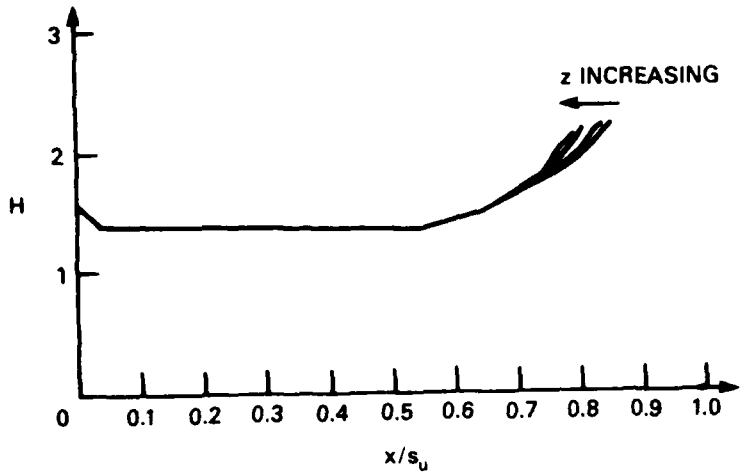

(a) D/h = 2.

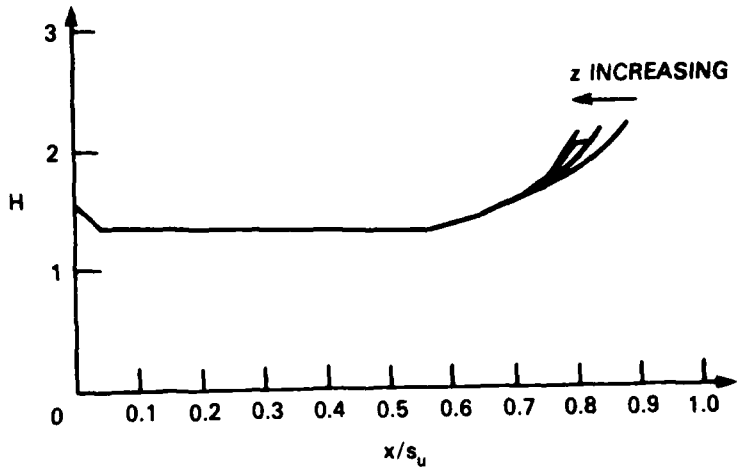

(b) D/h = 3.

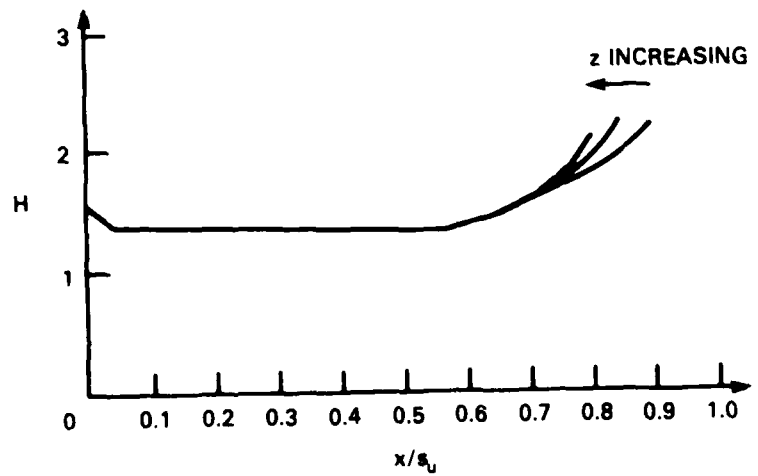

(c) D/h = 4.

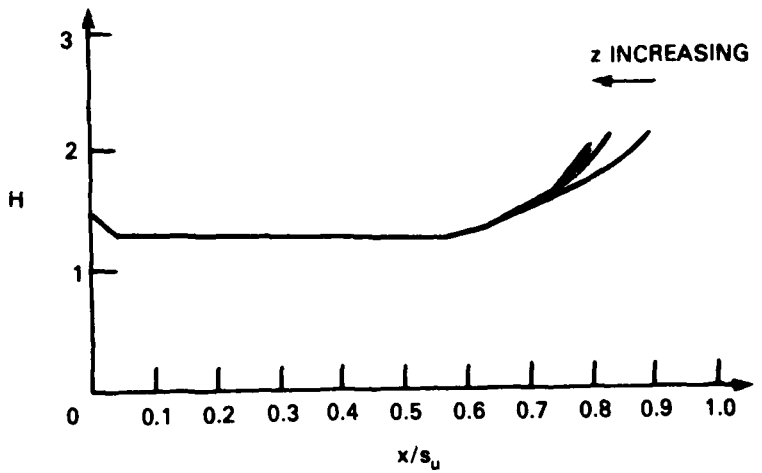

(d) D/h = 5.

(x_v/s_u = 0.4, h = 0.5 ft, α_v = 15°)

Fig. 12b. D/d = 3, c_v/h = 2.

Fig. 12. (Continued)

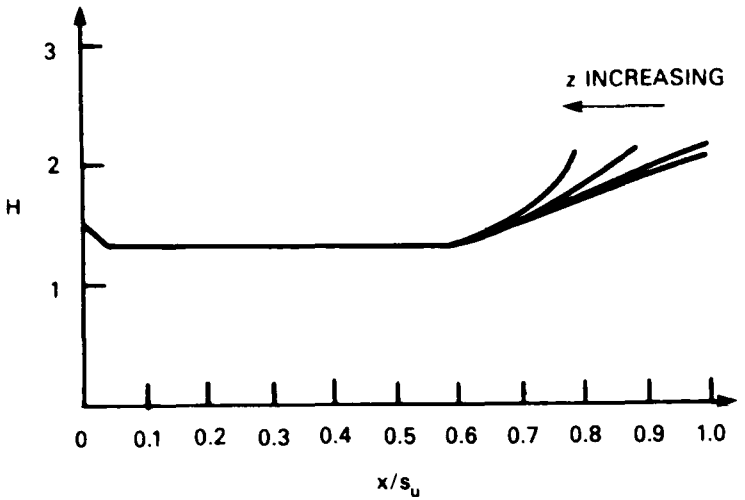

(a) D/h = 3.

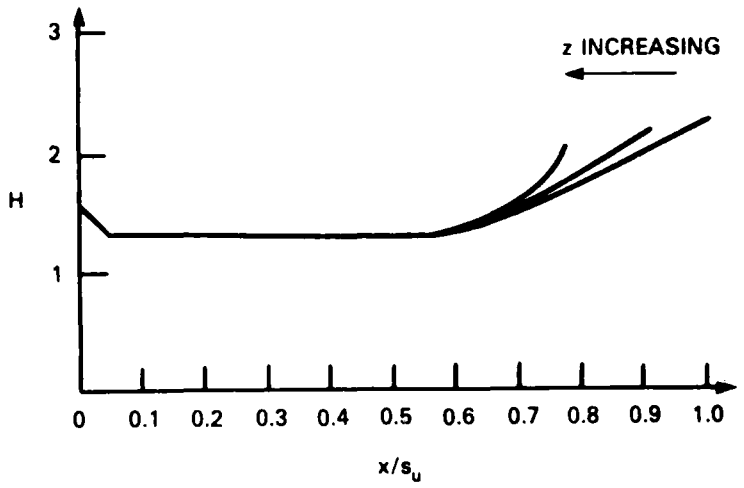

(b) D/h = 4.

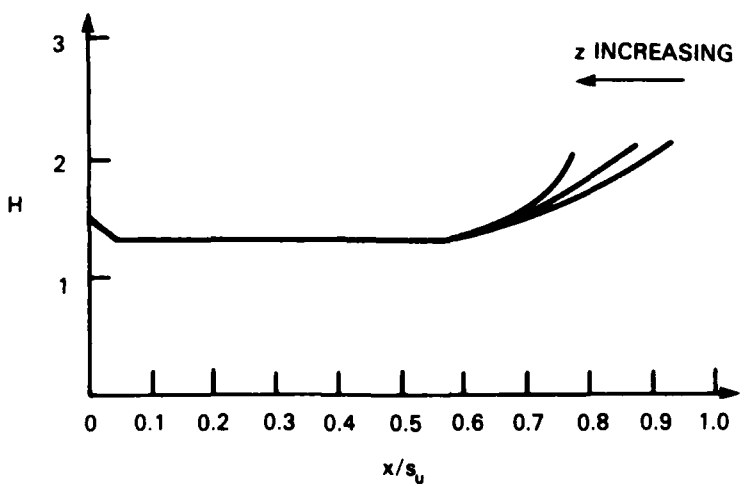

(c) D/h = 5.

(x_v/s_u = 0.4, h = 0.5 ft, α_v = 15°)

Fig. 12c. D/d = 2, c_v/h = 4.

Fig. 12. (Continued)

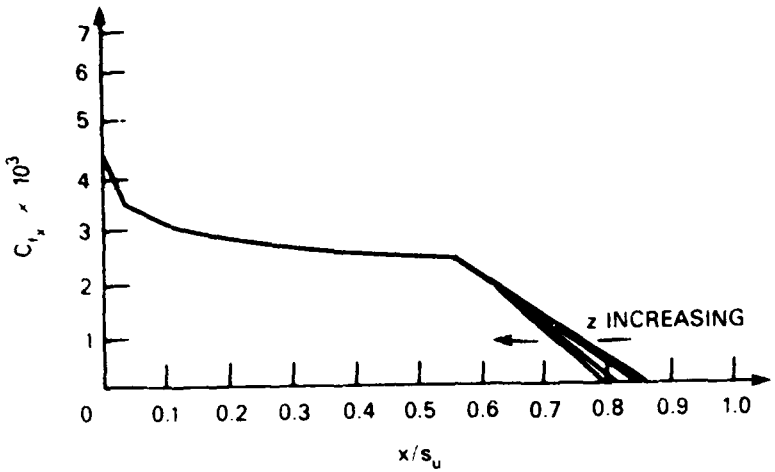

(a) D/h = 2.

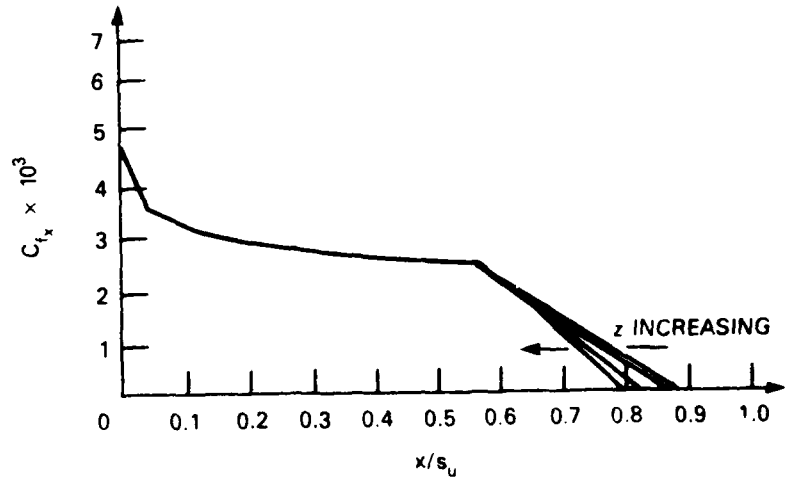

(b) D/h = 3.

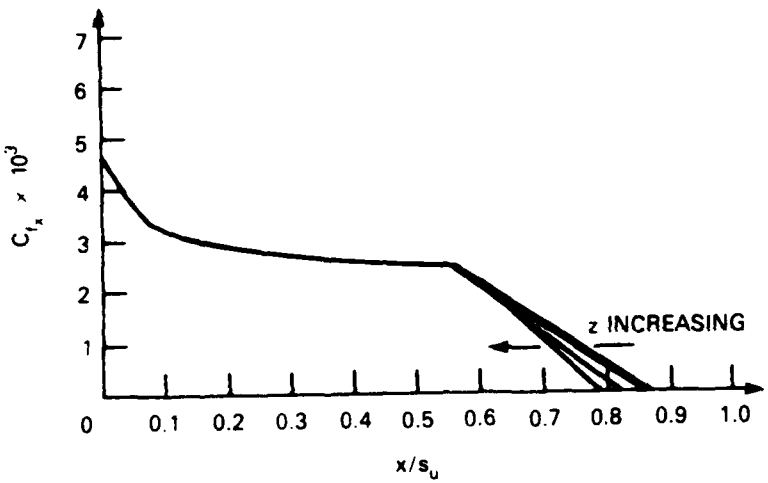

(c) D/h = 4.

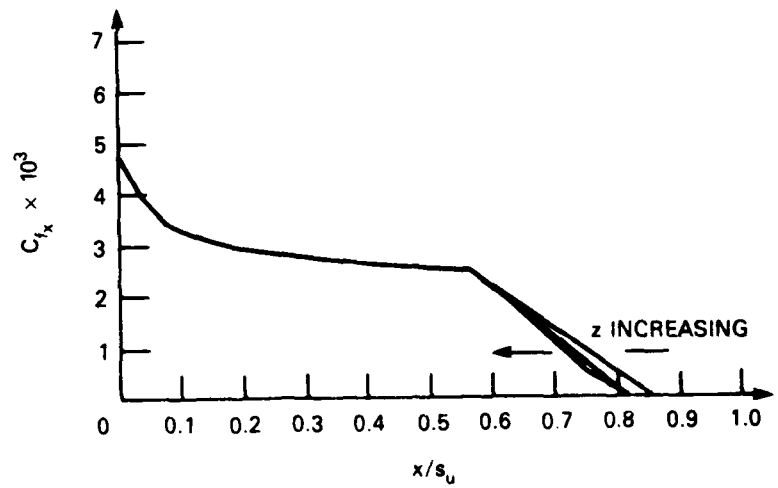

(d) D/h = 5.

(x_v/s_u = 0.4, h = 0.5 ft, α_v = 15°)

Fig. 13a. D/d = 2, c_v/h = 2.

Fig. 13. Skin friction coefficient C_{f_x} curve in parameter of z.

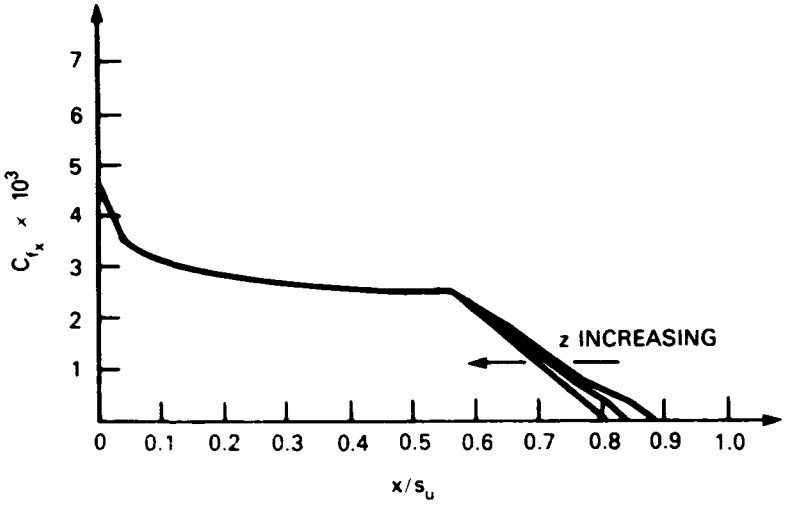

(a) D/h = 3.

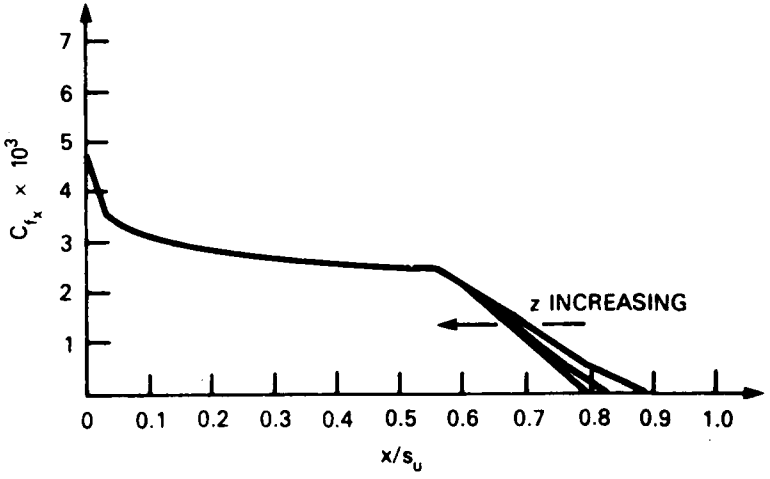

(b) D/h = 4.

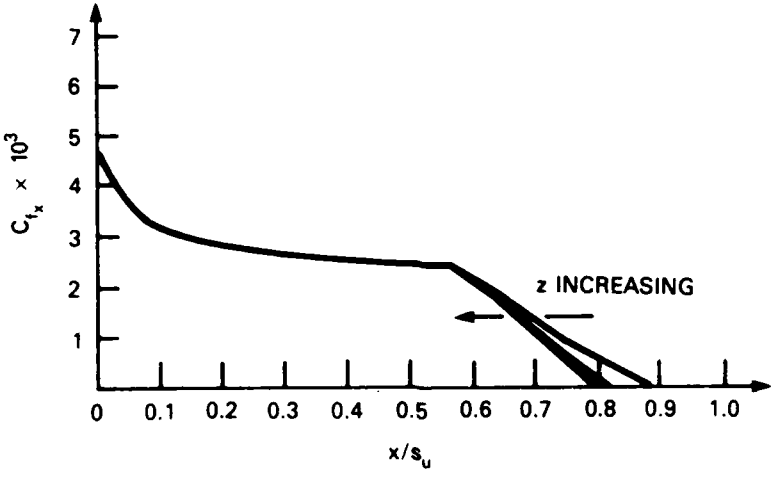

(c) D/h = 5.

(x_v/s_u = 0.4, h = 0.5 ft, α_v = 15°)

Fig. 13b. D/d = 4, c_v/h = 2.

Fig. 13. (Continued)

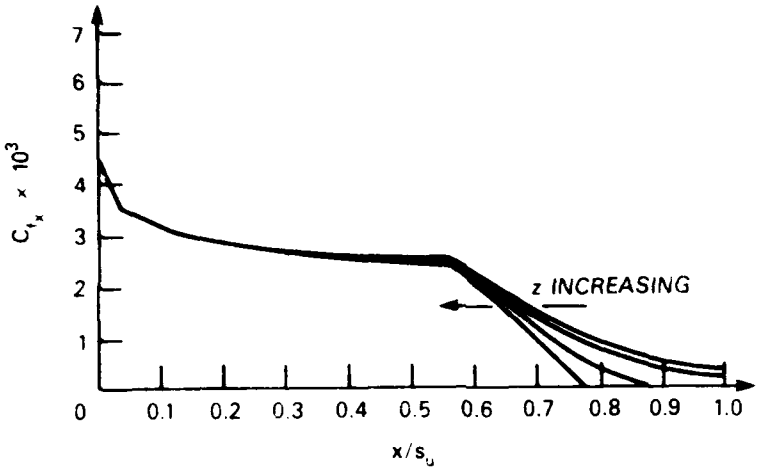

(a) D/h = 3.

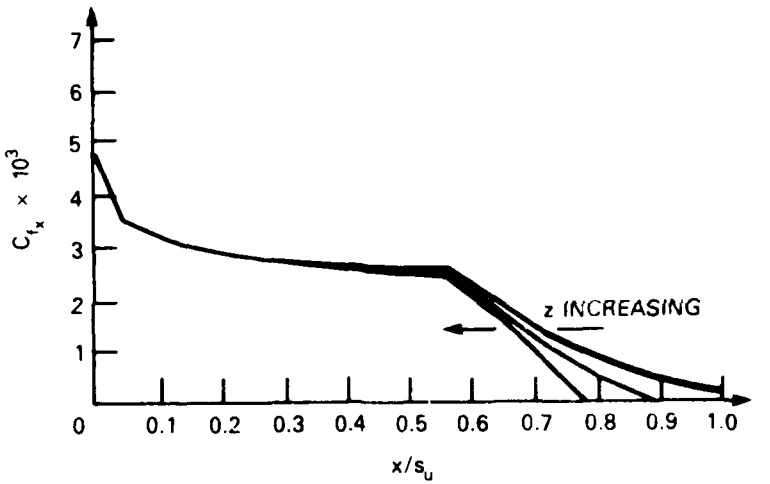

(b) D/h = 4.

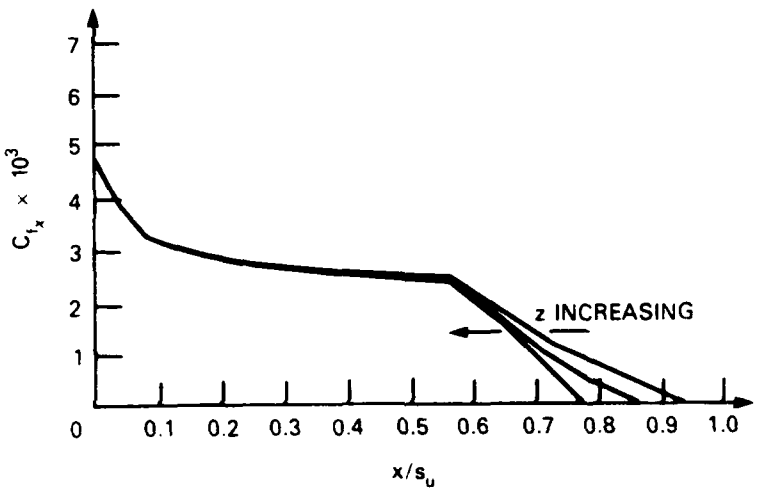

(c) D/h = 5.

(x_v/s_u = 0.4, h = 0.5 ft, α_v = 15°)

Fig. 13c. D/d = 2, c_v/h = 4.

Fig. 13. (Continued)

APPENDIX A

APPROXIMATE EVALUATION OF VORTEX STRENGTH OF VORTEX GENERATOR

The two-dimensional approximate analysis of Jones (1957)[3] is used to evaluate the vortex strength of the vortex generator; more details are given in Ref. 3. The induced angle of attack to the vortex generator blade is W/U_v. Thus the effective angle of attack to the blade at any point P is

$$\phi_v = \alpha_v - \frac{W}{U_v} .$$

The lift at any span-wise element dz is

$$\delta L_v = a \frac{\varrho}{2} \left\{ \alpha_v - \frac{W_m}{U_v} \right\} c_v \cdot U_v^2 \, dz$$

where a is the lift slope.

For convenience the mean value W_m is taken in order to apply the simple horseshoe vortex system of lifting line theory.

The Kutta-Joukowsky theorem gives

$$\delta L_v = \varrho U_v \Gamma \, dz.$$

Hence,

$$\Gamma = \frac{a}{2} \left\{ \alpha_v - \frac{W_m}{U_v} \right\} c_v \cdot U_v .$$

Letting

$$\gamma = \frac{\Gamma}{DU_v} = \frac{a}{2} \left\{ \alpha_v - \frac{W_m}{U_v} \right\} c_l ,$$

where

$$c_l = c_v / D$$

and D is the distance between the vortex generators shown in Fig. 3, and

$$W_m = \frac{\Gamma \lambda}{D} ,$$

the previous equation becomes

$$\gamma = \frac{\alpha_v}{\frac{2}{ac_l} + \lambda} .$$

The total strength of the trailing vortices behind any generator is assumed equal to the total circulation around that generator, i.e., around blade of height h.

Therefore, if c_v is used instead of D and γ' is defined by

$$\Gamma = \gamma' c_v U_v = \gamma D U_v \qquad \gamma' = \gamma \frac{D}{c_v} = \gamma \frac{1}{c_l}$$

$$\gamma' = \frac{\alpha_v}{\frac{2}{ac_l} + \lambda} \frac{1}{c_l}$$

$$\Gamma = \frac{\alpha_v}{\frac{2}{ac_l} + \lambda} \frac{1}{c_l} \cdot c_v \cdot U_v = \frac{\alpha_v c_v U_v}{\frac{2}{a} + c_l \cdot \lambda}$$

$$\lambda = \frac{W_m \cdot D}{\Gamma} = \frac{W_m D}{\Gamma c_v} \cdot c_v = \frac{c_v}{c_l} \frac{1}{h} \int_0^h \frac{W}{\Gamma} dy$$

for a given x and z. Hence,

$$\Gamma = \frac{\alpha_v \cdot c_v U_v}{\frac{2}{a} + \frac{c_v}{h} \int_0^h \frac{W}{\Gamma} dy} . \quad (a \approx 2\pi)$$

Therefore

$$\Gamma \approx \frac{\alpha_v c_v U_v}{\frac{1}{\pi} + \frac{c_v}{h} \int_0^h \frac{W}{\Gamma} dy}$$

or

$$\Gamma \approx \frac{\alpha_v h U_v AR_v}{\frac{1}{\pi} + AR_v \int_0^h \frac{W}{\Gamma} dy}$$

where

$$AR_v = c_v/h.$$

APPENDIX B

CEBECI AND SMITH TURBULENCE MODEL

Cebeci (Refs. 14, 22-24) proposed the following eddy-viscosity model:

$$\varepsilon = (\varkappa y)^2 \left[1 - \exp\left(-\frac{y^*}{A^*}\right)\right]^2 \sqrt{\left(\frac{\partial u}{\partial y}\right)^2 + \left(\frac{\partial w}{\partial y}\right)^2} \; ; \; 0 \leqslant y \leqslant y_c \text{ (Cebeci [1975]}^{22}\text{)}$$

$$\varepsilon = \alpha \left| \int_0^\infty (U_s - \sqrt{u^2 + w^2})\, dy \right| \left[1 + 5.5\left(\frac{y}{\delta}\right)^6\right]^{-1}; \; y_c < y. \text{ (Cebeci [1970]}^{23}\text{)}$$

Since ε is continuous, y_c is determined from these two equations, and the upper limit satisfies the law of wall $y^* = y\, u^*/\nu$. A^* is the Van Driest dampling factor given by

$$A^* = A_0/N$$

where

$$N = \sqrt{1 - 11.8\, p^*} \qquad p^* = -\frac{\partial p}{\partial s}\frac{\nu}{\varrho u^{*3}} \qquad \text{(Cebeci, Smith [1974],}^{14} \text{ pp. 214, 216, 217)}$$

$\frac{\partial p}{\partial s}$ is the pressure gradient along the stream line

$$u^* = \sqrt{\frac{\tau_w}{\varrho}} = \text{wall shear velocity}$$

$$\varkappa = 0.4 + \frac{0.19}{1 + 0.49\,\sigma^2}, \quad \sigma = Re_\theta \cdot 10^{-3} > 0.3 \text{ (Cebeci, Smith [1974],}^{14} \text{ p. 222).}$$

$$A_0 = 26 + \frac{14}{1 + \sigma^2}$$

$$\alpha = 0.0168 \qquad Re_\theta > 6000$$

$$\alpha = \frac{0.0168 \times 1.55}{1 + \Pi} \qquad 425 \leqslant Re_\theta < 6000 \qquad \text{(Cebeci [1973],}^{24} \text{ Cebeci, Smith [1974],}^{14} \text{ p. 224).}$$

$$\alpha = 10^{-3}\,(194.8 - 128.6 \times \log Re_\theta + 30.925 \times \log Re_\theta{}^2$$

$$-2.475 \times \log Re_\theta{}^3), \; Re_\theta < 425 \qquad \text{(Chang, Patel [1975]}^{16}\text{)}$$

where

$$Re_\theta = \frac{\theta\, U_s}{\nu}$$

$$\Pi = 0.55\ [1 - \exp(-0.243\ \gamma_t^{0.5} - 0.298\ \gamma_t)]$$

and $\gamma_t = (Re_\theta/425) - 1$ (Cebeci, Smith [1974],[14] p. 221)

APPENDIX C
COEFFICIENTS OF MOMENTUM EQUATIONS

$$\Delta x = x(i+1) - x(i),\ \Delta z = z(k) - z(k-1)$$

$$\Delta y_+ = y(j+1) - y(j),\ \Delta y_- = y(j) - y(j-1)$$

$$d_+ = \frac{h_x\,\Delta x}{\Delta y_+\,(\Delta y_+ + \Delta y_-)},\quad d_- = \frac{h_x\,\Delta x}{\Delta y_-\,(\Delta y_+ + \Delta y_-)}$$

$$r_1 = \frac{\bar{v}\,d_+\,\Delta y_-}{2\bar{u}},\quad r_2 = \frac{\bar{v}\,d_-\,\Delta y_+}{2\bar{u}},\quad r_3 = \frac{h_x\,\Delta x\,\bar{w}_z}{2\bar{u}}$$

$$s_1 = [1+\varepsilon(i+1,j+1/2,k)]\,d_+/\bar{u}$$

$$s_2 = [1+\varepsilon(i,j-1/2,k)]\,d_-/\bar{u}$$

$$s_3 = [1+\varepsilon(i,j+1/2,k)]\,d_+/\bar{u}$$

$$s_4 = [1+\varepsilon(i,j-1/2,k)]\,d_-/\bar{u}$$

$$s_5 = [1+\varepsilon(i+1,j+1/2,k-1)]\,d_+/\bar{u}$$

$$s_6 = [1+\varepsilon(i+1,j-1/2,k-1)]\,d_-/\bar{u}$$

$$s_7 = [1+\varepsilon(i,j+1/2,k-1)]\,d_+/\bar{u}$$

$$s_8 = [1+\varepsilon(i,j-1/2,k-1)]\,d_-/\bar{u}$$

$$t = \frac{\bar{w}\,h_x\,\Delta x}{\bar{u}\,\Delta z}$$

$$A(j) = -r_2 - s_2,\qquad C(j) = r_1 - s_1$$

$$B_1(j) = 1 + r_2 - r_1 + s_2 + s_1 + t$$

$$B_2(j) = 1 + r_2 - r_1 + s_2 + s_1 + t$$

$$B_3(j) = 1 + r_2 - r_1 + s_2 + s_1$$

$$B_4(j) = 1 + r_2 - r_1 + s_2 + s_1 + r_3$$

$$D_1(j) = \frac{\bar{U}}{\bar{u}}[U(i+1,k) - U(i,k) + U(i+1,k-1) - U(i,k-1)]$$

$$- \frac{h_x\,\Delta x\,\bar{W}}{\Delta z\,\bar{U}}[U(i+1,k) - U(i,k) - U(i,k-1) - U(i+1,k-1)]$$

$$+ (r_2 + s_4)\, u(i,j-1,k) + (1 + r_1 - r_2 - s_3 - s_4 + t)\, u(i,j,k)$$

$$- (-r_1 + s_3)\, u(i,j+1,k) + (r_2 + s_6)\, u(i,j-1,k-1)$$

$$+ (1 + r_1 - r_2 - s_7 - s_8 - t)\, u(i,j,k-1) + (-r_1 + s_7)\, u(i,j+1,k-1)$$

$$D_2(j) = \frac{\overline{U}}{\overline{u}}[w(i+1,k) - w(i,k) + w(i+1,k-1) - w(i,k-1)]$$

$$- \frac{h_x\, \Delta x\, \overline{W}}{\overline{U}}[w(i+1,k) + w(i,k) - w(i+1,k-1) - w(i,k-1)]$$

$$- (r_2 - s_4)\, w(i,j-1,k) - (1 + r_1 - r_2 - s_3 - s_4 - t)\, w(i,j,k)$$

$$+ (-r_1 + s_3)\, w(i,j-1,k) + (r_2 + s_6)\, w(i,j-1,k-1)$$

$$+ (1 + r_1 - r_2 - s_7 - s_8 - t)\, w(i,j,k-1) + (s_7 - r_1)\, w(i,j+1,k-1)$$

$$D_3(j) = \frac{\overline{U}}{\overline{u}}[U(i+1,k) - U(i,k)] + (r_2 + s_4)\, u(i,j-1,k)$$

$$+ (1 + r_1 - r_2 - s_3 - s_4)\, u(i,j,k) + (-r_1 + s_3)\, u(i,j+1,k)$$

$$D_4(j) = \frac{h_x\, \Delta x\, \overline{U}}{\overline{u}}\left[\frac{1}{h_x\, \Delta x}\,[w_z(i-1,k) - w_z(i,k)] + \frac{\overline{u}}{h_x\, \Delta x}\,\frac{\overline{W}_z{}^2}{\overline{U}}\right]$$

$$+ (r_2 + s_4)\, w_z(i,j-1,k) + (1 + r_1 - r_2 - s_3 - s_4 - r_3)\, w_z(i,j,k)$$

$$+ (-r_1 + s_3)\, w_z(i,j-1,k)$$

Superscript — is space averaged; $\overline{u}$, $\overline{v}$, $\overline{w}$, and $\overline{w}_z$ are assumed to be known by projecting the velocity profile at the station (i,j,k) forward to station (i + 1,j,k) for all y and k according to

$$V(i+1,j,k) = \frac{V(i+1,n+1,k)}{V(i,n+1,k)}\, V(i,j,k).$$

APPENDIX D

GEOMETRICAL ARRANGEMENT OF VORTEX GENERATORS

Schopper* investigated the problem of determining the maximum chord length c_v which, for a given D/h and D/d, does not result in the blades crossing. The term c_v/h is evaluated as a function of $(D/h)/(D/d) = d/h$.

a. Self-crossing

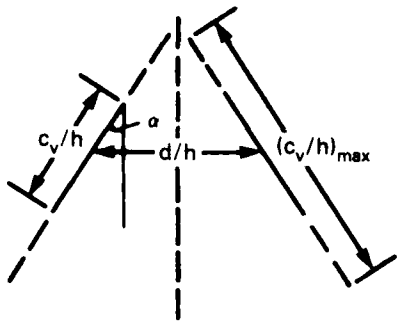

For a given d/h, self-crossing occurs when

$$(c_v/h)_{max} = \frac{d/h}{\sin \alpha} . \qquad (40)$$

For no self crossing,

$$c_v/h < (c_v/h)_{max}$$

b. Interference.

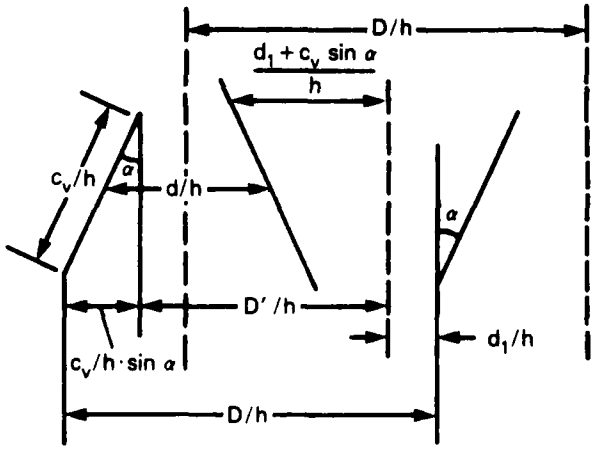

The condition for no interference between pairs is

$$\frac{D'}{h} > \frac{d_1 + c_v \sin \alpha}{h}$$

$$\frac{d_1}{h} = \frac{1}{2}\frac{d - c_v \sin \alpha}{h}$$

$$\frac{D'}{h} = \frac{D - d_1 - c_v \sin \alpha}{h} .$$

Then

$$\frac{D - d_1 - c_v \sin \alpha}{h} > \frac{d_1 + c_v \sin \alpha}{h}$$

or

$$\frac{D}{h} > \frac{d + c_v \sin \alpha}{h}$$

or

$$\frac{c_v}{h} < \frac{D - d}{h}\frac{1}{\sin \alpha} .$$

*Private communication with M.R. Schopper, David Taylor Research Center.

For no interference,

$$\frac{c_v}{h} < \frac{d}{h} \frac{1}{\sin \alpha} \frac{D}{d} - 1 \tag{41}$$

From Eqs. 40 and 41 and $D/d > 2$, c_v/h is determined by Eq. 40. Examples of $(c_v/h)_{max}$ are shown in the following table for several values of D/d and D/h at α_v = 15 degrees, i.e., $1/\sin \alpha_v = 3.864$:

D/d	D/h = 2		D/h = 3		D/h × 4		D/h = 5		D/h = 10	
	d/h	$(c_v/h)_{max}$	d/h	$(c_v/h)_{max}$	d/h	$(c_v/h)_{max}$	d/h	$(c_v/h)_{max}$	d/h	$(c_v/h)_{max}$
2	1	3.864	1.5	5.796	2	7.728	2.5	9.66	5	19.32
3	2/3	2.576	1	3.864	4/3	5.15	5/3	6.44	10/3	12.88
4	1/2	1.932	3/4	2.898	1	3.804	5/4	4.83	2.5	9.66
5	2/5	1.546	3/5	2.318	4/5	3.09	1	3.864	2	7.728

REFERENCES

1. Schubauer, G.B. and W.G Spangenberg, "Forced Mixing in Boundary Layers," *J. of Fluid Mech.*, Vol. 8, pp. 10-32 (1960).
2. Brown, A.C., et al., "Subsonic Diffusers Designed Integrally with Vortex Generators," Paper 67-464, AIAA Third Propulsion Joint Specialist Conference, Washington, D.C. (Jul 17-21, 1967).
3. Jones, J.P., "The Calculation of the Paths of Vortices from a System of Vortex Generators and a Comparison with Experiment," Aeronautical Research Council C.P. 361 (1957).
4. Pearcey, H.H., "Shock Induced Separation and Its Prevention by Design and Boundary Layer Control," Vol. 2, *Boundary Layer and Flow Control*, Lachmann, G.V., Ed., Pergamon Press (1961).
5. Gartling, D.K., "Test of Vortex Generators to Prevent Separation of Supersonic Flow in a Compression Corner," ARL-TR-70-44, Applied Research Laboratories, The University of Texas, Austin, Texas (1970).
6. Senoo, Y. and M. Nishi, "Improvement of the Performance of Conical Diffusers by Vortex Generators," *J. of Fluid Eng.*, Transaction of the ASME, pp. 4-10 (Mar 1974).
7. Nickerson, J.D., "A Study of Vortex Generator at Low Reynolds Numbers," AIAA 24th Aerospace Sciences Meeting, Reno, Nevada (Jan 1986).
8. Greene, G.C., "An Approximate Model of Vortex Decay in Atmosphere," *J. of Aircraft*, Vol. 23, No. 7 (1986).
9. Lee, Ill Woo, "Analysis of Alleviation of Flow Separation in the Symmetrical Plane of Thick Airfoil with Vortex Generators at Subsonic Speed," Korea Advanced Institute of Science and Technology, Seoul, Korea (1986).
10. Lugt, H.J., *"Vortex Flow in Nature and Technology,"* John Wiley & Sons (1983).
11. Widnall, S.E., "The Structure and Dynamics of Vortex Filaments," Annual Review of Fluid Mechanics, Vol. 7, Ed. M. Van Dyke, Annual Review, Inc., Palo Alto, California (1975).
12. Nash, J.F. and V.C. Patel, "Three-Dimensional Turbulent Boundary Layers," SBC Technical Books, Scientific and Business Consultants, Inc., Atlanta, Georgia (1972).
13. Chen, K.K. and N.A. Thyson, "Extension of Emmon's Spot Theory to Flows on Blunt Bodies," *AIAA J.*, Vol. 9, pp. 821-825 (1971).
14. Cebeci, T. and A.M.O. Smith, *"Analysis of Turbulent Boundary Layers,"* Academic Press, pp. 234-239, New York (1974).
15. Schlichting, H., *"Boundary Layer Theory,"* McGraw-Hill Book Co., New York, pp. 79-83 (1960).
16. Chang, K.C. and V.C. Patel, "Calculation of Three-Dimensional Boundary Layers of Ship Forms," IIHR Report 178, Iowa Institute of Hydraulic Research, The University of Iowa (1975).

REFERENCES (Continued)

17. Klinksiek, W.F. and F.J. Pierce, "A Finite Difference Solution of the Two- and Three-Dimensional Incompressible Turbulent Boundary Layer Equations," *J. of Fluid Eng.*, Transactions of the ASME, pp. 445-458 (Sep 1973).

18. Schopper, M.R., "Airfoil Generation with a Desktop Computer Using Lighthill's Exact Inverse Method," Paper AIAA-83-1967, AIAA Applied Aerodynamics Conference, Danvers, Massachusetts (Jul 13-15, 1983).

19. Lighthill, M.J., "A New Method of Two-Dimensional Aerodynamic Design," Aeronautical Research Council R&M 2112, pp. 105-157 (1945).

20. Wang, K.C., "Three-Dimensional Boundary Layer Near the Plane of Symmetry of a Spheroid at Incidence," *J. of Fluid Mech.*, Vol. 43, Part 1, p. 207 (1970).

21. Cebeci, T., K.C. Chang, R.W. Clark, and D. Sedlock, "Applications of Two- and Three-Dimensional Interactive Boundary Layer Theory to Finite Wings with Flow Separation," AIAA Paper 87-0590, Presented at AIAA 25th Aerosciences Meeting, Reno, Nevada (Jan 12-15, 1987).

22. Cebeci, T., "Calculation of Three-Dimensional Boundary Layers—II. Three-Dimensional Flows in Cartesian Coordinates," *AIAA J.*, Vol. 13, No. 8, pp. 1056-1064 (1975).

23. Cebeci, T. et al., "Calculation of Compressible Adiabatic Turbulent Boundary Layers," *AIAA J.*, Vol. 8, No. 11, pp. 1974-1982 (1970).

24. Cebeci, T., "Kinematic Eddy Viscosity at Low Reynolds Numbers," *AIAA J.*, Vol. 11, No. 1, pp. 102-104 (1973).

INITIAL DISTRIBUTION

Copies

- 2 CONR
  - 1 Tech Lib
  - 1 Code 1132F
- 1 NSWC/Tech Lib
- 1 NWC/Tech Lib
- 1 NAVAIRSYSCOM
  - 1 AIR-931
  - 1 AIR-931M
- 2 NAVSEA/SEA-99612/Tech Lib
- 1 DARPA
- 12 DTIC
- 1 BRL, Aberdeen/Tech Lib
- 1 AFOSR/Aero Science
- 1 AFWAL/Tech Lib
- 1 AFFDL/Tech Lib
- 1 AEDC/Tech Lib
- 1 NASA STIF/Baltimore
- 1 NASA Ames Res Cen
- 1 NASA Langley Res Cen
- 1 NASA Lewis Res Cen
- 1 NSF/Tech Lib
- 1 U of Arizona/Lib
- 1 Calif Inst of Tech/Grad Aero Labs
- 2 U of Calif, Berkeley
  - 1 Lib
  - 1 M. Hold/Div Aero Sciences
- 1 U of Calif, Davis/Lib
- 1 U of Calif, Los Angeles/Lib

Copies

- 3 Catholic U of America
  - 1 Lib
  - 1 A.G. Favret/Engr & Arct
  - 1 W. Kelnhofer/Mech Engr
- 1 Case Western Reserve U
- 2 U of Cincinnati
  - 1 Lib
  - 1 Aerospace Eng
- 1 U of Colorado/Lib
- 2 Cornell U
  - 1 D.A. Caughey/Mech Aero
  - 1 S.F. Shen/Mech Aero
- 1 George Washington U/Lib
- 1 Georgia Inst Tech/Aerospace Engr
- 1 Johns Hopkins U/APL/Tech Lib
- 2 U of Maryland
  - 1 Aerospace Engr
  - 1 J.D. Anderson, Jr.
- 2 MIT
  - 1 Lib
  - 1 E.M. Murman/Dept Aero
- 2 N Carolina State U, Raleigh
  - 1 Lib
  - 1 F.R. DeJarnette/Mech &Aero Eng
- 1 Notre Dame U/Lib
- 1 Ohio State U/Lib
- 1 Pennsylvania State U/Lib
- 1 Princeton U/Lib
- 1 Purdue U/Lib
- 1 Rensselaer Polytech Inst/Lib

Copies	
1	Rutgers State U/Lib
2	San Diego State U
	1 Lib
	1 K.C. Wang Mech Engr
2	U of Southern Calif
	1 Lib
	1 H.K. Cheng; Aero Dept
1	Stanford U/Lib
2	U of Tennessee Space Inst
	1 Lin
	1 C.M. Wu
2	Virginia Polytech Inst State U
	1 Carol M. Newman Lib
	1 Aero & Ocean Engr
1	American Inst of Aero & Astro
1	Calspan Corp/Tech Lib
1	Douglas Aircraft Co, Long Beach/Lib
1	Flow Research, Kent, WA/Lib
1	Grumman Aerospace Corp/R. Melnik
1	Lockheed-Georgia/Tech Lib
1	LTV Aerospace Corp, Dallas/Tech Lib
2	McDonnell-Douglas Helicopters, Inc, St. Louis
	1 MCAIR
	1 MDRL
1	Neilsen Engr & Res Inc/Tech Lib
1	Scientific Res Assoc, CT/ Tech Lib
1	United Technology Res Ctr, CT/Tech Lib

CENTER DISTRIBUTION

Copies	Code	Name
1	0113	F. Halsell
1	0117	B. Nakonechny
1	15	W.B. Morgan
1	16	H.R. Chaplin
1	166	J.H. Nichols
1	166.3	T.C. Tai
3	166.4	Aerodynamics Collection
10	5211.1	Reports Control
1	522.1	TIC (C)
1	522.2	TIC (A)
1	9300	Patent Counsel

DTNSRDC ISSUES THREE TYPES OF REPORTS:

1. **DTNSRDC reports, a formal series,** contain information of permanent technical value. They carry a consecutive numerical identification regardless of their classification or the originating department.

2. **Departmental reports, a semiformal series,** contain information of a preliminary, temporary, or proprietary nature or of limited interest or significance. They carry a departmental alphanumerical identification.

3. **Technical memoranda, an informal series,** contain technical documentation of limited use and interest. They are primarily working papers intended for internal use. They carry an identifying number which indicates their type and the numerical code of the originating department. Any distribution outside DTNSRDC must be approved by the head of the originating department on a case-by-case basis.

END

DATE

FILMED

5-88

DTIC